

24818431



This is to certify that the

dissertation entitled

Quantitative Investigations of Neuronal Architecture

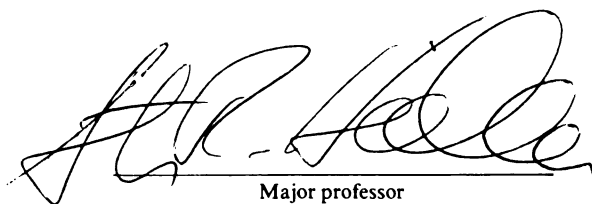
and the Structural Role of the Cytoskeleton

presented by

Timothy John Denner11

has been accepted towards fulfillment
of the requirements for

Ph.D. degree in Physiology

A handwritten signature in black ink, appearing to be "H. P. Keller", written over a horizontal line.

Major professor

Date June 8, 1989

PLACE IN RETURN BOX to remove this checkout from your record.
TO AVOID FINES return on or before date due.

DATE DUE	DATE DUE	DATE DUE
_____	_____	_____
_____	_____	_____
_____	_____	_____
_____	_____	_____
_____	_____	_____
_____	_____	_____
_____	_____	_____

MSU Is An Affirmative Action/Equal Opportunity Institution

QUANTITATIVE INVESTIGATIONS OF NEURONAL ARCHITECTURE
AND THE STRUCTURAL ROLE OF THE CYTOSKELETON

By

Timothy John Dennerll

A DISSERTATION

Submitted to
Michigan State University
in partial fulfillment of the requirements
for the degree of

DOCTOR OF PHILOSOPHY

Department of Physiology

1989



6001877

ABSTRACT

QUANTITATIVE INVESTIGATIONS OF NEURONAL ARCHITECTURE AND THE STRUCTURAL ROLE OF THE CYTOSKELETON

By

Timothy John Dennerll

The elastic properties of PC-12 neurites were assessed by applying force with a calibrated glass needle for 1-2 seconds and measuring the resulting changes in neurite length and needle deflection. We observed a linear relationship between neurite tension and length change and were thus able to determine neurite spring constants and initial rest tensions. We observed positive neurite rest tensions ranging over three orders of magnitude but clustering around 30-40 microdynes. Treatment with an anti-actin drug reduced neurite rest tensions while treatment with an anti-microtubule drug increased tensions. These observations suggest a complementary force interaction underlying axonal shape: the cortical actin network under tension and the microtubule core under compression.

We also used force-calibrated glass needles to measure PC-12 neurite lengthening in response to experimentally applied tensions over time periods of 30-60 minutes. We found that initial applied tensions of 100 microdynes or less caused a two phase, viscoelastic neurite length increase. This behavior is modelled with a trio of



classical mechanical elements: two springs and a dashpot. Computer simulations based on the expected behavior of this model closely match experimental observations. At applied tensions of greater than 100 udynes, there is an additional third phase of elongation with an average rate linearly dependent on applied force. We tentatively interpret this third phase to be towed axonal growth as observed by Bray. In the presence of 1 μM taxol, only the third elongation phase is inhibited, suggesting its dependence upon microtubule assembly.

The viscosity of F-Actin and microtubule suspensions was measured as a function of shear rate with a Weissenberg rheogoniometer. At shear rates of less than 1.0 sec^{-1} the viscosity of suspensions of these two structural proteins is inversely related to shear rate. These results are consistent with previous in-vivo measurements of the viscosity of cytoplasm. This power law implies that shear stress is independent of shear rate; that is, shear stress is a constant at all shear rates less than 1.0 sec^{-1} . This flow property may explain several aspects of intracellular motility in living cells. Possible explanations for this flow property are based on a recent model for semidilute suspensions of rigid rods or a solid friction model for liquid crystals.

DEDICATION

To my father Donald Dennerll, who taught me to be critical in thinking, so that I might not be fooled into settling for anything but the truth.

To my mother Jane Weiser, who believed I could achieve any goal I set my heart on and thus gave me the courage to be successful.

To my wife Jeanie, a princess who spied a frog in the pond and kissed him so that he might become a man.

To my daughter Diane, who instructs me daily in the important things in life and is definitely the best stinker I know.

To my son Raymond, whose smile melts my heart every day.

ACKNOWLEDGMENTS

Mom, Jerry, Dad and Evie, because of the terminology, you may find the meaning of the rest of this dissertation to be somewhat less than clear. Yet I'm sure that you appreciate the amount of work it represents. My success is no accident; it is the result of my being supported and coached by many outstanding people. Along the way I discovered something quite remarkable, that each one of us wants to make a contribution to another, but we usually aren't willing to be contributed to. Learning how to let myself be supported has been one of the most valuable (and necessary) discoveries I made during my graduate program. I also want you all to know that through this experience (as well as my becoming a parent myself), I have become deeply aware of your love for me, and the knowledge that this was the source of what I feel to be my greatest strength: my love for myself and God which in turn sources my ability to contribute to the lives of those around me.

I am unable to acknowledge either my wife Jeanie or my advisor Steve Heidemann enough for their commitment to my success, one that many times exceeded my own and without which I would have given up long ago. Steve, you have been a true mentor to me in many ways. Your enthusiasm for your work has inspired me to try to be my very best. I especially thank you for greeting me like the prodigal son after my disappearances; it allowed me to begin to trust others in helping me find my way. Jeanie, your patience and willingness to support me through school during almost our entire marriage so far has meant more to me than you'll ever know, I only hope that I will have the opportunity to return this gift to you some day.

I'm very lucky to have Robert Buxbaum as both an advisor and friend. Bux, you have clearly made it possible for me to successfully pursue my interest in physics in a biological setting. I also thank my other committee members Ron Meyer, Mel Schindler and Birgit Zipser for their thoughtful contributions to my education and this dissertation. Other faculty I would like to acknowledge are Sherwood Haynes, Seth Hootman, Jack Krier, Clarence Suelter, Lynne Weaver, and John Wilson.

There are many other people whom I have come to call friends and would like to thank for their support. In particular I wish to acknowledge Greg Adams, Peter Baas, Mary Lynn Bajt, Jean Foley, Harish Joshi, Phil Lamoureux, Jerry Lepar, Charles Liang, Shelly Maiorana, Vivian Steel, Leigh White, and Jing Zhen.

There is one more person who I need to acknowledge for her love and support which has gone far beyond the call of duty. Helen, you have made it possible for me to have it all. I truly appreciate your partnership in caring for our children as well as the many delicious meals, washed clothes and house cleanings. I also thank you for giving me such a beautiful and charming daughter for my wife.



TABLE OF CONTENTS

List of Figures	vii
General Introduction	1
Chapter 1. Quantitative Measurements of Tension and Compression in the Cytoskeleton of PC-12 Neurites.	
Introduction	7
Materials and Methods	9
Results	13
Discussion	26
Chapter 2. Tension, Viscoelasticity, and Growth in PC-12 Neurites.	
Introduction	31
Materials and Methods	33
Results	35
Discussion	48
Chapter 3. F-Actin and Microtubule Suspensions as Indeterminate Fluids.	
Introduction	55
Materials and Methods	56
Results and Discussion	58
Appendix A. Method for analytical determination of neurite mechanical constants from observed distension behavior.	71
Appendix B. Logic underlying the computer simulation based on our viscoelastic model for neurite distension.	72
List of References	78

LIST OF FIGURES

Figure 1.	Method of measurement of neurite tension by lateral displacement.	11
Figure 2.	Three typical plots of neurite axial tension vs. change in neurite length.	14
Figure 3.	Frequency distribution for neurite rest tensions.	15
Figure 4.	Frequency distribution for neurite spring constants.	17
Figure 5.	Neurite tension as a function of length change before and after addition of 0.1% DMSO.	19
Figure 6.	Neurite tension as a function of length change before and after addition of 2 ug/ml cytochalasin D.	21
Figure 7.	Summary of the effect of cytochalasin D on neurite rest tension.	22
Figure 8.	Neurite tension as a function of length change before and after addition of 1 ug/ml nocodazole.	23
Figure 9.	Summary of the effect of nocodazole on neurite rest tension.	24
Figure 10.	Method of measurement of neurite tension during long duration distension.	34
Figure 11.	Neurite length and tension as a function of time for a 2-phase neurite distension.	36
Figure 12.	Viscoelastic model of neurite mechanical response to long duration distension.	38
Figure 13.	Computer simulation of observed neurite distensions using our viscoelastic model.	39
Figure 14.	Computer simulation of hypothetical neurite distensions.	40

Figure 15.	Neurite length and tension as a function of time for a 3-phase neurite distension.	42
Figure 16.	Low and high initially applied tensions on the same neurite.	43
Figure 17.	Threshold tension for phase 3 neurite elongation.	45
Figure 18.	Taxol inhibition of phase 3 neurite elongation.	46
Figure 19.	3-position controller model for the tension dependence of neurite length.	52
Figure 20.	Viscosity as a function of shear rate for F-actin and microtubule suspensions.	59
Figure 21.	Effect of shear history on viscosity of F-actin.	61
Figure 22.	Viscosity of F-actin compared with viscosity measurements of cytoplasm by various in-vivo methods.	62
Figure 23.	Shear stress as a function of shear rate for cytoskeletal proteins and the viscosity standard.	64
Figure 24.	Polarization micrographs of suspensions of actin and microtubules.	70

INTRODUCTION

Fundamental to the design of all structures is a strategy to resist deformation and collapse from forces that originate both externally from the surrounding environment and internally from active and passive processes. Both the mechanical properties of materials used as well as the manner in which individual elements are structurally related bear on this problem. Unlike most man-made structures which are composed of solid, static elements, the living cell is structurally dynamic at both the organizational and molecular levels (2). In addition and probably in part as a result, the cell seems to behave mechanically with both 'solid-like' and 'fluid-like' properties (44,46,73,80).

The shape, polarity, and motility of all eucaryotic cells is thought to be the result of the organization and control of the cell's cytoskeleton (2). This "cell skeleton" is generally considered to be composed of three filamentous protein polymers: F-actin, microtubules and intermediate filaments. Although the cytoskeleton is presumed to provide the structural support for the cell, very little work has been done to describe mechanical behavior or the architectural role for individual cytoskeletal elements. Towards a better understanding of these problems, this dissertation attempts to explore the following basic questions. What are the mechanical properties of the cell at the level of individual elements

and in complete integrated structures? How is the cytoskeleton organized in supporting both internal and external forces such that it is able to determine and maintain cell shape?

There is convincing evidence that external force plays a role in determining cell shape, polarity, and motility. A wide variety of cell types have been clearly shown to exert force on their environment (6,39,107). Some of the forces exerted by cells are involved in the crawling movement and stationary shape of cells (1,39). There is widespread agreement that these forces must be generated and supported by the cellular cytoskeleton (107). External force applied to many cells has a major effect on their morphology and motile behavior. Perhaps best known is the work of Bray (11) who has shown that axonal growth can be elicited by experimentally applied mechanical tension. Vandenburg (110) has shown that chick skeletal myofibers will orient themselves to tension applied while the cells are growing. Also experimentally applied tensile stress causes an increase in the migratory activity of isolated corneal epithelia of embryonic chick (104).

Neurons make good models for investigating the role of the cytoskeleton in determining cell shape, polarity, and motility. These cells develop their highly asymmetric shape through a tip growth process: an advancing growth cone appears to initiate the formation of both axons and dendrites. The importance of the cytoskeleton in



determining neuronal motility and elongation is widely accepted (13,60,63,84,108). The available evidence (55,60) suggests that axonal elongation may be divided into two phases; 1) actin based forward motility of the growth cone and 2) actin and microtubule based elongation of the axon. There is widespread agreement that the axon elongates as a result of a "pulling" growth cone (10,11,60,63,84,108). In particular, Bray has provided convincing evidence that tension on the neurites (processes of cultured neurons) is sufficient to cause their elongation. He showed that the vector sum of all neurite segments of a single cultured neuron nearly always formed a closed loop, indirectly indicating that the cell body was suspended by a network of neurites under tension (9). In addition, using a "towing motor" attached to the growth cone, he was able to "pull out" a morphologically and ultrastructurally normal neurite (11). This suggests that the integrative coupling between growth cone movement and axonal elongation is solely one of mechanical force. Campenot (20) observed cell body movements when neurites either elongated or shortened. He similarly concluded that nerve fiber elongation is normally controlled by tension generated by growth cone movements. In further support, Letourneau (61) showed that neurites will preferentially navigate into regions of greater adhesivity. In light of Bray's findings that neurites could be guided by tension alone (9), Letourneau (62) reinterpreted his 1975 findings as a tensile competition between weaker and

stronger adhesion sites. That is, the greater tension supported by the stronger adhesion breaks the weaker adhesions, and thus directs the growth cone to the more adhesive surface. In summary, both phases of axonal growth are thought to be dependent on the organization and function of the cytoskeleton. These experiments suggest that external force plays a role in the regulation of the axonal cytoskeleton during axonal elongation.

The structural organization of the cytoskeletal elements within the axon should reflect the forces they support. Previous work from our lab as well as other's have shown that anti-cytoskeletal drugs reveal a complementary "division of labor" within the neurite cytoskeleton. Anti-microtubule drugs cause the neurite to collapse but have little effect on the ruffling activity of the growth cone (14,27,40,51,53,98). Conversely, anti-actin drugs inhibit growth cone motility but neurites remain extended (14,40,53,98). In addition, drugs that disrupt actin networks stabilize the neurite to retraction, while drugs that disrupt microtubules cause retraction (53,65,98). These complementary drug effects may reflect a complementary force interaction in the neurite cytoskeleton: an actin network in tension supported in part by microtubule compression and in part by compression of the underlying substrate.

This dissertation is composed of three chapters, each one aimed at quantitatively measuring the relationship

between mechanical force and deformation of the cell or cytoskeleton. I was interested in investigating both the structural properties of individual elements and the structural relationships between them. The first two chapters deal with quantitative force measurements made at the cellular level on PC-12 neurites using force calibrated glass needles. This work has significance regarding both cytoskeletal architecture and neurobiology. For short duration deformations a classical Hookian 'solid-like' behavior is observed, allowing the quantitative measurement of both neurite tensions and spring constants. With the aid of microtubule and actin inhibitors, the complementary structural roles of these two cytoskeletal elements is confirmed: actin in tension and microtubules in compression. In the second chapter, long duration distensions are used to uncover some additional 'fluid-like' behaviors of the cell. This allows neurite structure to be modeled from classical mechanical elements: springs and dashpots. In addition, a tension induced neurite elongation, similar to the growth response observed by Bray (11), was observed and found to have a minimum force threshold, with elongation rate linearly related to applied force.

The elastic and viscoelastic measurements discussed in the first two chapters concern the mechanical behavior of the combined structural elements in the living cell. Toward a better understanding of this behavior, we also investigated the mechanical behavior of individual elements.



Cytoplasmic structure has long been thought to be a key element in understanding cell structure and motility (96,2). Recent investigators have focused on suspensions of the purified cytoskeletal filaments, because these suspensions (particularly of actin filaments) are found to have many of the properties of cytoplasm. Both cytoplasm and filament suspensions are shear thinning (71,79,88,89,119,120,). An initial stress "overshoot", indicative of a gel to sol transition, is also generally observed in both cytoplasm (26,90,109) and actin suspensions (71,79,88). Chapter 3 investigates the rheological properties of F-actin and microtubule suspensions to obtain a clearer understanding of cytoplasmic structure. This is done by measuring the forces associated with varying rates of shear applied to these suspensions. Surprisingly, all rates of shear produced the same amount of force for a particular sample. This unusual result is consistent with the combined force measurements made by others in-vivo on cytoplasm and provides some insight into the mechanics of cytoplasmic structure and cell motility.

CHAPTER 1. Quantitative Measurements of
Tension and Compression in the
Cytoskeleton of PC-12 Neurites.

INTRODUCTION

Since the pioneering studies of Yamada et al (117), many investigators have found a clear cut "division of labor" in the role of the cytoskeleton in growth cone motility and axonal elongation. Anti-microtubule drugs cause neurites to collapse but have no effect on growth cone motility functions, eg. ruffling, microspike activity, etc. (14,27,40,51,53,98). Conversely, anti-actin drugs inhibit growth cone motility functions but neurites remain extended (14,40,53,98). Further, drugs that disrupt the actin network stabilize the neurite to retraction, while drugs that disrupt microtubules (MTs) cause retraction. Also, drugs that augment actin assembly cause retraction while drugs that augment MT assembly stabilize neurites to retraction and sometimes cause extension (24,53,65,98). Similarly, the networks move at different rates in slow axonal transport (8). Apparently, while microtubule-based and actin-based elements of neuronal growth interact, they are structurally and functionally distinct (60).

Neurites of cultured neurons have been shown by indirect means to be under tension (9,53). Bray (11) elicited apparently normal neurite elongation by "towing"

neurites with an appropriately paced motor in a process very similar to the "towed growth" long known to occur in situ (112). Tension has also been shown to markedly alter the motility at the edge of fish skin cells (57), align the division plane of plants (67) and dramatically orient growing chick myofibers (110). These and other examples (107) of mechanical force affecting cell growth, shape and polarity, processes widely regarded to depend on cytoskeletal function (2,28), suggest that tension may play a role in regulating the cytoskeleton. Previous results from our lab (53) caused us to propose that actin and microtubules in PC-12 neurites are in a complementary force interaction: the actin network being under tension that is partly supported by microtubule compression and partly supported by the underlying substrate. This postulated complementary force interaction, similar to the interaction of structural elements in "tensegrity" architecture (34), provides, in principle, a means for integrating microtubule assembly with the advance of the growth cone.

In an effort to better understand the structural roles of actin and microtubules in axonal shape and to test our complementary force model, we directly measured mechanical force in PC-12 neurites and the effect of cytoskeletal drugs on that force.



MATERIALS AND METHODS

Cell Culture

PC-12 cells were grown as previously described (53), primed in 50 ng/ml 7s nerve growth factor (NGF) for 4-6 d, then replated on untreated 60 mm tissue culture dishes in 7s NGF media, allowing neurites to regenerate for 2-3 days prior to tension measurements. The microscope was mounted on a vibration isolation table and cultures were maintained at 37°C on the microscope stage with an air curtain incubator (Sage Instruments, Jamaica Plains, MA). Nocodazole (Aldrich Chemical Co., Inc., Milwaukee WI) and cytochalasin D (Sigma Chemical Co., St. Louis, MO) stock solutions were prepared at 1000x concentration in DMSO (Sigma Chemical Co., St. Louis, MO), with final experimental concentrations of 1 ug/ml nocodazole and 2ug/ml cytochalasin D with 0.1% DMSO for each. Neurite tensions were measured (see below) both prior to and 10-15 mins following addition of drug. Only those neurites that remained attached throughout an experimental series of deflections could be analyzed for the effect of the drug. Drug treated neurites showed length changes of less than 5%, generally less than 1%. Control experiments were done in a similar manner in 0.1% DMSO.



Force Needle Calibration

Glass needles were fabricated and calibrated for force as described by Nicklas (78), with the following modifications. Two relatively stiff "reference" needles were made from 8 and 16 mm lengths of uniform diameter 25 μm chromel wire (Omega Engineering, Inc., Stamford, CN). Each was calibrated for force by hanging weights from their tips. A third 24 mm wire needle could then be calibrated indirectly by using the following standard relation from beam theory: $\text{Force} = (\text{constant})(\text{tip displacement})/(\text{needle length})^3$. Values obtained for the constant from the two shorter (stiffer) needles differed by less than 1% and gave a calculated value of 90.9 udynes/ μm deflection for the third needle. More flexible glass needles were then calibrated by bending them against this wire needle, and subsequently glass needles against each other, to get "working" needles with stiffness calibration constants (Cal) of 1-10 udynes/ μm .

Neurite Tension Measurement

To make a tension measurement, a force calibrated needle is placed at the center of the neurite and rapidly moved perpendicular to the neurite axis, using a Narishige hydraulic micromanipulator, causing both neurite distension and needle deflection (see figure 1). After holding for 2-3 secs, the needle is lifted; both needle and neurite assume rest positions almost instantaneously. This procedure is

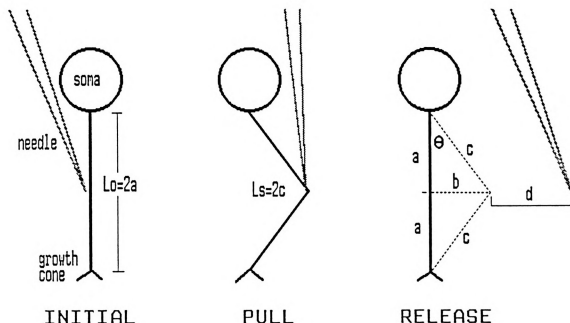


Figure 1. Method for measurement of neurite tension by lateral displacement.

A force calibrated glass needle is placed at the neurite center (left), micromanipulated orthogonal to the neurite axis and held for 1-2 seconds (center), and then lifted allowing the neurite to straighten and the needle tip to assume its equilibrium position (right). Following the experiment, measurements are made from recorded video images of neurite rest length (L_0), neurite lateral displacement (b) and force calibrated needle deflection (d). These measurements are used to calculate neurite axial tension and change in neurite length (see Materials and Methods).

repeated 10 to 20 times at various displacements in random order. Video recording allows direct measurement from the video screen of neurite rest length (L_0), lateral neurite displacement (b), and needle deflection (d) for each "pull". Screen measurements were converted into actual distances through the use of a stage micrometer. These values were used to calculate axial neurite stretch tension (T_s) in udynes and corresponding neurite stretch lengths (L_s) for each pull by the following analysis: Since $c^2 = a^2 + b^2$, $L_s = 2c = 2\sqrt{a^2 + b^2}$. A vector force balance is then used to determine axial forces in the stretched neurite:

$$T_s = T_0 + k_1(L_s - L_0) = \text{force parallel to neurite axis}$$

$$d(\text{Cal}) = \text{force perpendicular to neurite}$$

$$d(\text{Cal}) = 2\sin\theta(T_0 + k_1(L_s - L_0))$$

$$\sin\theta = b/c = 2b/L_s$$

$$d(\text{Cal}) = 4b(T_0 + k_1(L_s - L_0))/L_s \quad T_0 = \text{neurite rest tension}$$

$$d(\text{Cal})L_s/4b = T_0 + k_1(L_s - L_0) \quad k_1 = \text{neurite spring constant}$$

Distended neurite axial tension $d(\text{Cal})L_s/4b$ is plotted as a function of change in neurite length ($L_s - L_0$). Linear plots indicate Hookian elastic behavior where the y-intercept equals the neurite rest tension (T_0 , tension at zero distension) and the slope equals the spring constant (k_1).

RESULTS

Neurites are Under Tension

PC-12 neurites were multiply distended in a direction orthogonal to the neurite axis using a force calibrated glass needle to measure neurite mechanical properties (see figure 1 and materials and methods). Tensions were measured on 82 neurites and figure 2 shows the results for three typical tension experiments. Regression coefficients (R) of 0.80 or better were observed in over 90% of the neurite length-tension plots. Initial neurite rest lengths varied between 34 and 176 μm , and maximum strains varied between 4.1% and 16.6% of the initial rest length. The y-intercept of the length-tension plot represents the tension on the neurite with no displacement (neurite rest tension, T_0) and the slope is the neurite spring constant (k_1). The observed rest tensions for 82 neurites varied over 3 orders of magnitude (see figure 3) but most neurites exhibited rest tensions in the neighborhood of 35 udynes, and only 1 rest tension value was less than zero (~ 2 udynes). We found no correlation between neurite length and rest tension. Interestingly, we found a visual cue that correlates to neurite rest tension. A small roughly spherical bleb in the neurite just proximal to the growth cone is typically associated with low observed rest tensions (1-25 udynes). This bleb becomes more ovoid in shape in neurites with intermediate rest tensions (25-200 udynes), disappearing



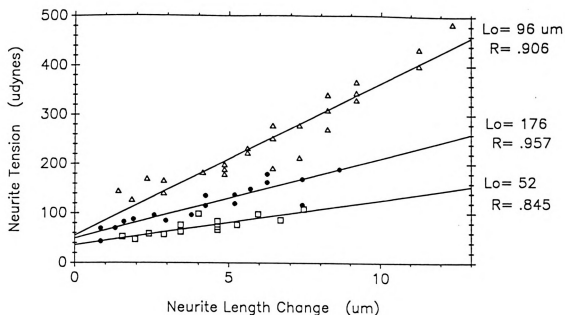


Figure 2. Three typical plots of neurite axial tension vs. change in neurite length.

Neurite axial tension calculated as described in material and methods is plotted as a function of neurite length change. Each data point represents a single "pull" as shown in figure 1. Straight lines were fitted to the data by a least squares fit regression. In all such plots, the slope of the line represents neurite spring constant (k_1) and the y-intercept indicates the tension on the neurite with no displacement (neurite rest tension, T_0).



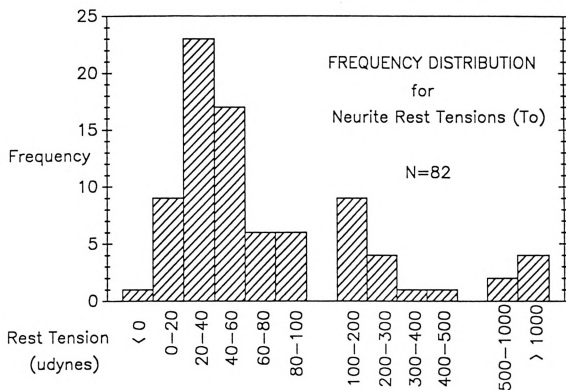
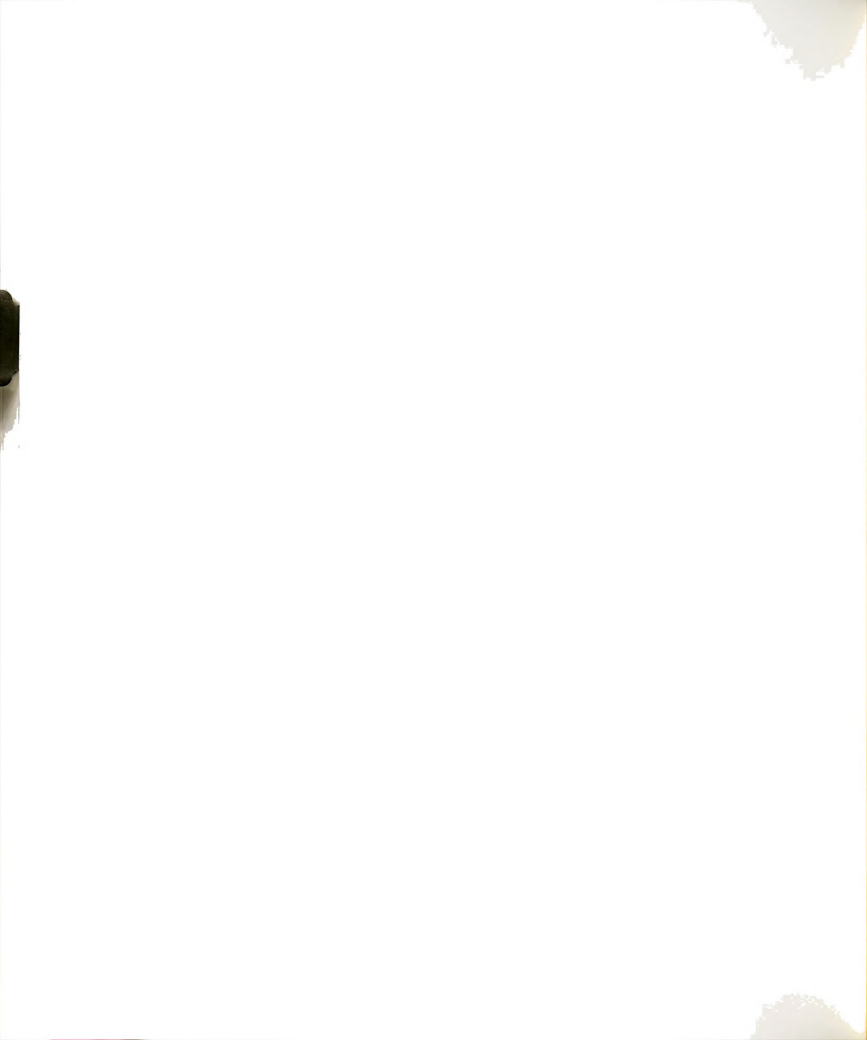


Figure 3. Frequency distribution for neurite rest tensions. Summary of results for 82 neurite rest tensions derived from plot intercepts as in figure 2.



into the neurite body at greater rest tensions. The highest observed tensions (1-3 millidynes) are comparable to those observed in the first cleavage furrow of the echinoderm egg (85).

Neurite spring constants varied over a narrower range than rest tensions. Figure 4 shows the frequency distribution for spring constants for 75 of the 82 measured neurites. The mean value was 24.4 ± 2.2 (std. error) udynes/um with 85% of values falling between 5 and 40 udynes/um. The 7 neurites not included here were those very high tension neurites for which we were unable to obtain accurate spring constant measurements. There was no significant correlation between spring constant and neurite length or tension.

Control Treatment

Experiments involved multiple distensions before and after treatments with anti-cytoskeletal drugs dissolved in DMSO at a final concentration of 0.1%. As control experiments for the effects of DMSO and multiple distensions, we compared length-tension plots before and after treatment with DMSO. We initially deflected neurites various distances in random order to give an untreated reference line. A typical series of 15-20 "pulls" on a neurite would last 3 mins. DMSO was added to the culture dish to a final concentration of 0.1% and allowed to sit for 10-15 mins. The same neurite was then subjected to an



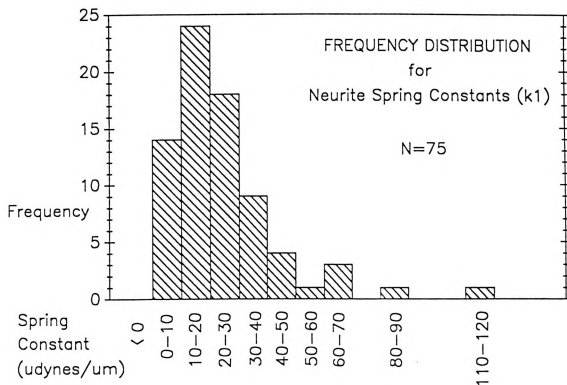


Figure 4. Frequency distribution for neurite spring constants.

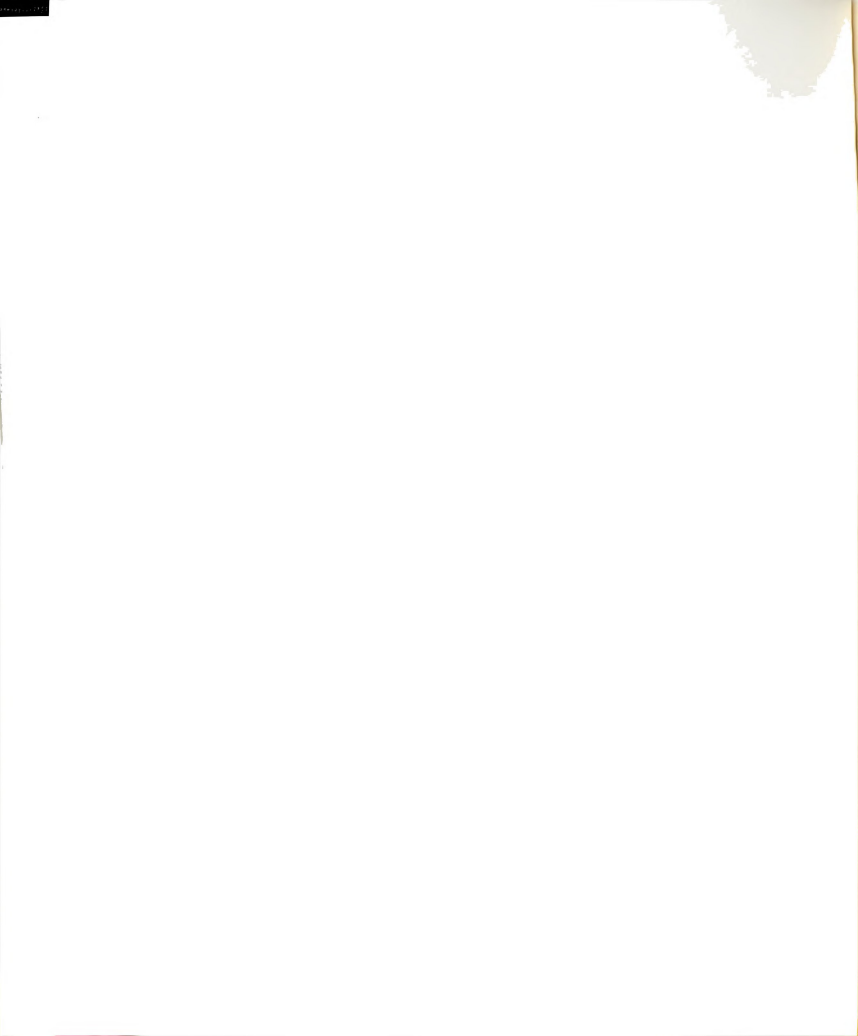
Summary of results for 75 neurite spring constants derived from plot slopes as in figure 2.



additional 15-20 pulls of random distensions for comparison with the above. Figure 5 is typical of these control experiments. Both within and between series of distensions, equal displacements produced nearly identical tension measurements. However, regression lines varied somewhat between pre- and post-DMSO plots producing small differences in rest tensions (y-intercept) and spring constants (slope). In 8 experiments, we found that rest tensions following DMSO treatment varied within 50% of their pre-treatment values; the average result was 99.8% of their pre-treatment rest tensions. Similarly, the spring constants averaged 110% of their reference values following DMSO treatment. Measurements from three neurites subjected to two bouts of multiple distensions fifteen minutes apart but without DMSO were indistinguishable from those with added DMSO. We conclude that neither the DMSO carrier nor the distensions themselves significantly affected the neurite mechanical properties measured.

Cytochalasin Reduces Neurite Tension

We tested the effect of the anti-actin drug cytochalasin D (16,45) on the neurite mechanical properties. Following a reference series of distensions, neurites were treated with 2 ug/ml cytochalasin D (Cyt-D) for approximately 10 mins. After treatment, additional series of random deflections were carried out on the same neurite. Figure 6 shows the results of such a Cyt-D experiment, with



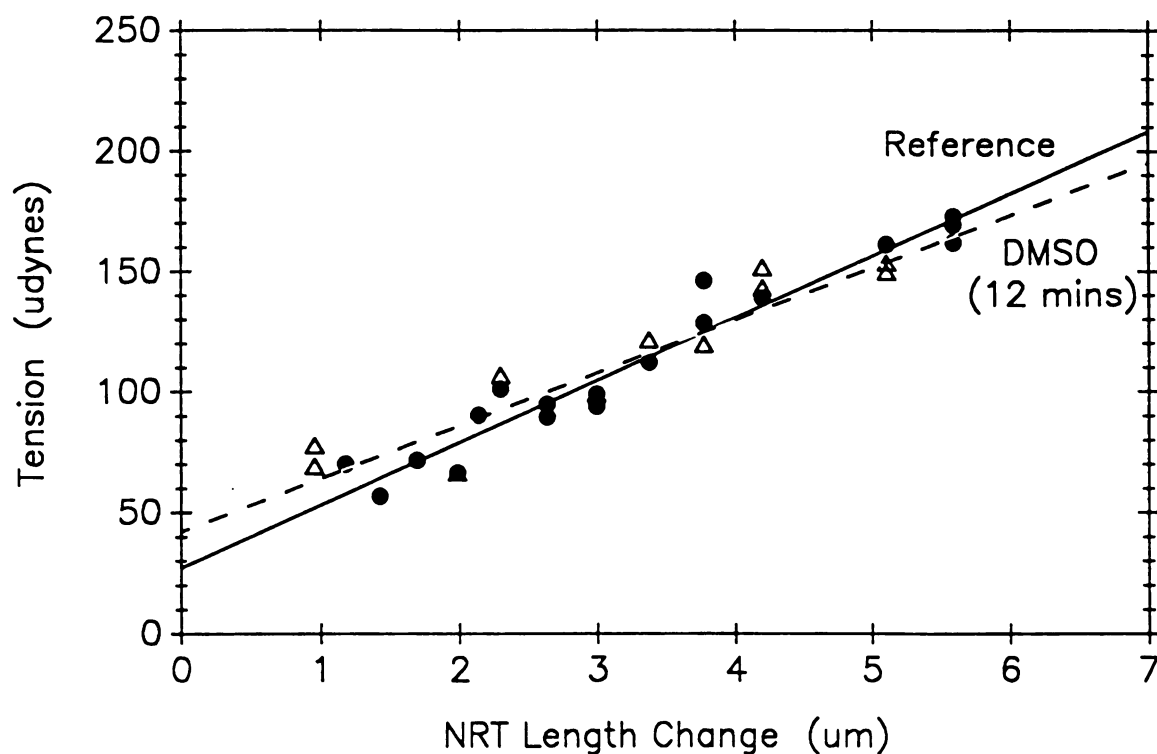
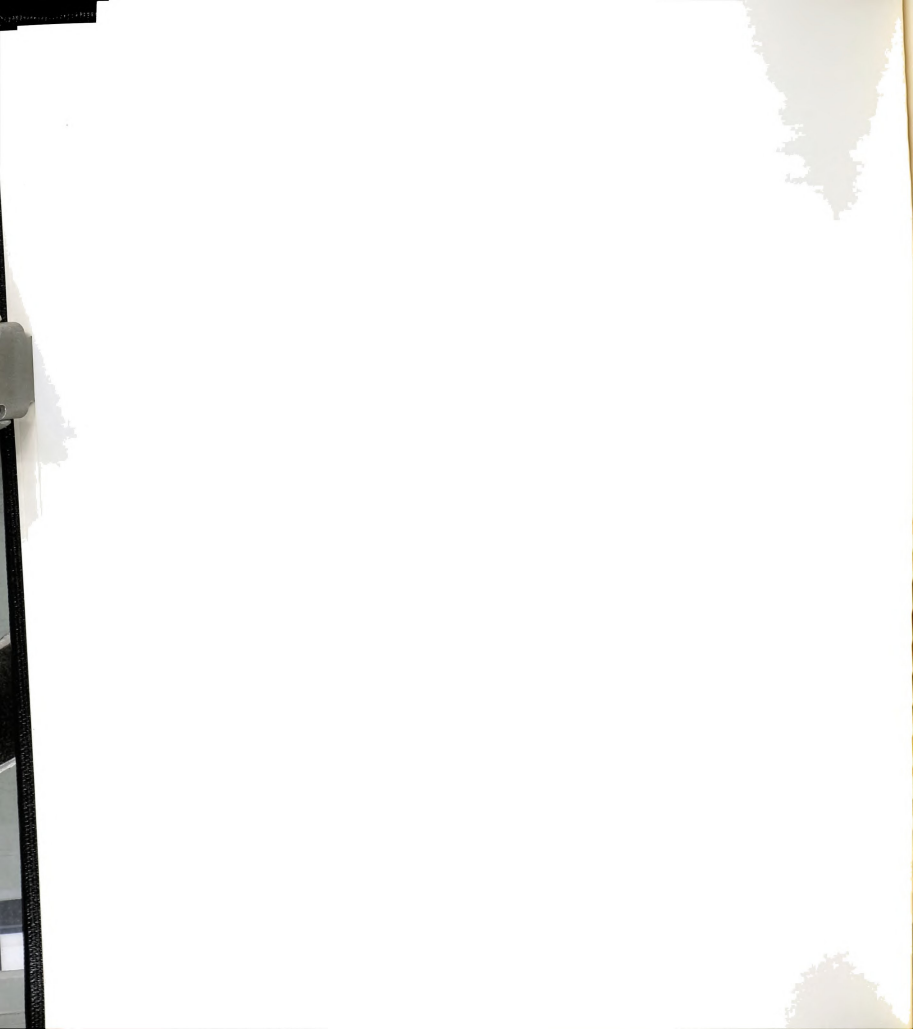


Figure 5. Neurite tension as a function of length change before (●) and after (Δ) addition of 0.1% DMSO (Control Experiment).

Neurite axial tension was plotted as a function of neurite length change (see figure 2) for 2 series of displacements on the same neurite.



one pre-treatment plot and two plots showing the effect of Cyt-D at 10 and 16 mins. As shown in this figure, the neurite rest tension and spring constant declined with increasing time of drug treatment. However, it was not possible to wait for a steady state value because the neurite behavior became primarily viscous and does not recover from distension. As summarized in figure 7, all Cyt-D treated neurites showed significant declines in rest tension; the maximum rest tension was 31.6% of the reference value. In two cases (including fig. 6) rest tension values following Cyt-D treatment fell below zero indicating a net neurite compression. The average result for all 7 neurites was a 114% decline in the initial rest tension, indicating net neurite compression. The neurite spring constants also declined, from a mean 15.2 udynes/ μ m to 2.4 udynes/ μ m after cytochalasin treatment, 15.8% of the reference value.

Nocodazole Increases Neurite Tension

We also tested the effect of the anti-microtubule drug nocodazole (29) on the neurite mechanical properties. Following a reference series of deflections, neurites were treated with 1 μ g/ml nocodazole (NOC) for approximately 10 mins followed by an additional series of random deflections on the same neurite. Figure 8 shows the results of a typical NOC experiment, with one pre-treatment plot and one plot showing the effect of NOC at 11 mins. As summarized in figure 9, all NOC treated neurites showed an increase in



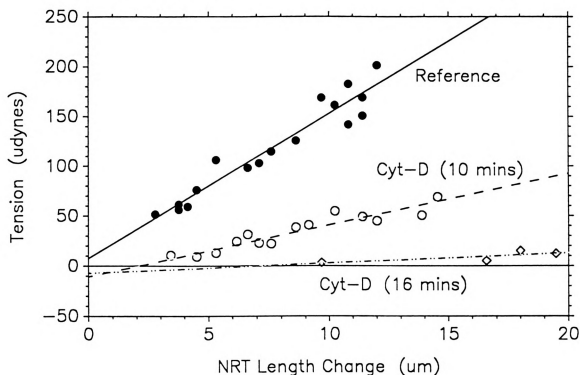


Figure 6. Neurite tension as a function of length change before (●), 10 minutes after (○) and 16 minutes after (◇) addition of 2 $\mu\text{g/ml}$ cytochalasin D.

Neurite axial tension is plotted as a function of neurite length change (see figure 2) for 3 series of displacements on the same neurite. In this trial, growth cone detachment ended the last series of displacements after 4 pulls. This is neurite #6 in figure 7.



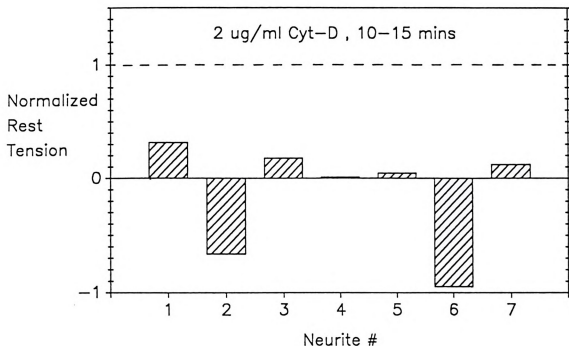


Figure 7. Summary of the effect of cytochalasin D on neurite rest tension.

The effect of cytochalasin D on rest tension is plotted for each of 7 neurites. The initial rest tension for each neurite is normalized to 1 and the graph shows the relative change for that neurite's rest tension after 10-15 mins drug exposure.



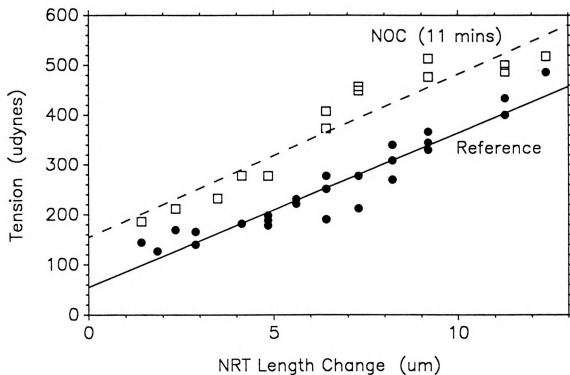


Figure 8. Neurite tension as a function of length change before (●) and after (□) addition of 1 ug/ml nocodazole.

Neurite axial tension is plotted as a function of neurite length change (see figure 2) for 2 series of displacements on the same neurite. This is neurite #8 in figure 9.

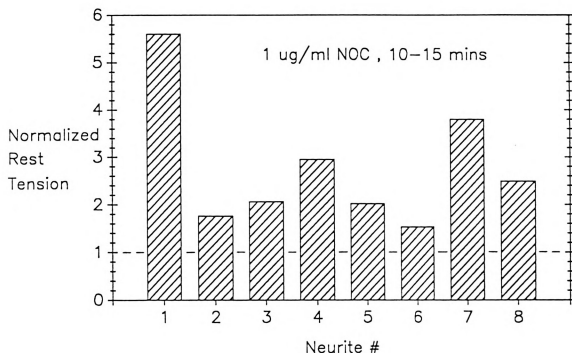


Figure 9. Summary of the effect of nocodazole on neurite rest tension.

The effect of nocodazole on neurite rest tension is plotted for each of 8 neurites. The initial rest tension for each neurite was normalized to 1 and the graph shows the relative change for that neurite's rest tension after 10-15 mins drug exposure.



rest tension ranging from 153% to 560% of the reference rest tension with an average value of 282%. These values appeared to be short lived plateaus; all neurites eventually retracted in response to the increased tension. However the neurite spring constants did not show a consistent change: four went up, two went down and two remained the same. The shift in the mean was negligible, going from a reference value of 20.5 udynes/um to 20.0 udynes/um in the drug treated neurites.

DISCUSSION

We found that growing neurites of PC-12 behaved as simple elastic solids for short duration distensions (2-3 secs). That is, we consistently found a linear relationship between applied force (axial tension) and the induced length change, and a high degree of reproducibility in measured force in multiple trials of the same distension (figure 2). In the presence of anti-cytoskeletal drugs, the linear regression coefficients decreased somewhat. This may reflect time dependent changes in spring constants during drug treatment of the neurites. As expected from observations of other cells (47,73,80,81), neurites behave viscoelastically under longer duration distensions.

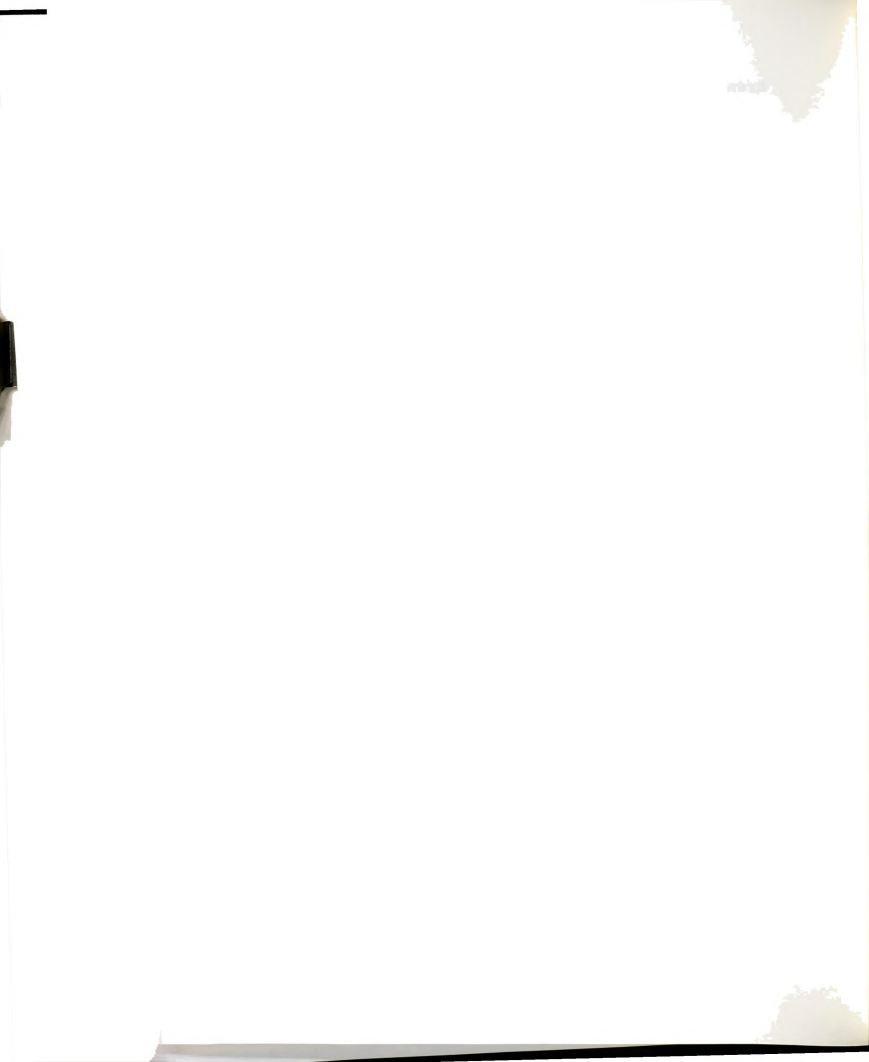
The majority (67%) of our measurements reported in figures 3 and 4 and all of our drug experiments were on isolated, non-branching neurites with active, filopodia bearing growth cones attached to the dish. We observed 23 such neurites for 30 min and found an average rate of elongation of 5.3 $\mu\text{m/hr}$, supporting the premise that this population is in an active growth phase. The remaining tension measurements were on neurites that terminated on other cells (23%), those that did not have visible filopodial activity (9%) and branched neurite segments (1%). Measurements from these neurites were indistinguishable from the majority of tension measurements. The most highly selected neurites were those which survived nocodazole



treatment. Most PC-12 neurites retract after treatment with nocodazole (40,53) but this tendency can be decreased (4,51) by allowing neurite outgrowth for periods longer than the 24 hours used previously (40,53). Approximately 30% of the cells regrown for 2-3 days and subjected to reference distensions remained extended long enough after nocodazole treatment to allow an additional series of distensions.

Direct mechanical measurements reported here confirm the hypothesis that neurites are under tension (9,53). The rest tension values were greater than zero in all but 1 of 82 growing neurites (figures 2 & 3). Clearly, the maintenance of this tension requires structural support. Our ability to measure a net tension in the highly asymmetric neurite at its "rest" length indicates that there is some tensile element in the neurite itself, and that this tension is at least partially supported externally, i.e. by compression of the dish. We are unable to interpret the wide range of observed neurite rest tensions (figure 3) at this time. However, experiments in progress should enable us to determine whether rest tension is related to some other variable such as neurite circumference, cortical actin network cross sectional area (Albrecht-Bühler, pers. comm.), total cross sectional area (9) and/or rate of elongation (6).

Neurite rest tensions may be manifestations of "surface forces" or "cortical tensions" observed by others in a variety of cell types (3,22,44,73,80,81,95). Cortical



tension may be the passive result of an osmotic force, an occasionally activated "motor" (15) or could be actively generated continuously within the cortical actin network (3,15). Alternatively, the neurite tension may be the passive result of tension generated by the growth cone (12,16,20,60,65,108). Although we do not know the source of the tension, we assume for a number of reasons that the measured tension is held passively. Previous results indicate that combined inhibitors of glycolysis and oxidative phosphorylation do not affect neurite retraction in PC-12 (31). The majority of evidence in neurons supports a pulling growth cone and we are unaware of studies suggesting continuously generated cortical force in neurites. Also, the assumption of continuously generated tension requires a number of ad hoc assumptions, not needed for passive tension models, to explain the tension changes following drug treatments. Passive tension allows us to interpret the effect of drugs by a simple force balance between elastic cytoskeletal elements; actin filaments and microtubules being measurably elastic in vitro (75,118).

Direct mechanical measurements demonstrate (figures 6 & 7) that cytochalasin D significantly reduces neurite rest tension. This indicates that anti-actin drug-sensitive elements are in tension. We presume the drug-sensitive structure correlates with the highly crossed-linked, actin-rich subplasmalemmal region of neurites (47,94). Addition of cytochalasin D disrupts actin networks in vivo (23,92)



dissipating tension in the network. If microtubules (MTs) are providing internal compressive support (53), their depolymerization should transfer additional tension support to the dish causing an increase in rest tension. Indeed, our measurements before and after depolymerization of MTs by nocodazole (29) demonstrate a significant increase in neurite rest tension in the presence of nocodazole (figures 8 & 9), supporting our claim that MTs are in compression and lending support to our previous claim (53) that nocodazole causes neurite retraction by increasing tension. The existence of an internal compressive support in the neurite is also suggested by the two cases where neurite rest tension fell below zero (and became a positive compression) in the presence of cytochalasin D. Under conditions of stationary neurite attachment to a stationary substrate, the change in neurite force from net tension to net compression indicates that some internal element is under compression. Based on changes in cell shape caused by cytoskeletal drugs, chick embryo fibroblasts grown in collagen matrix appear to have a similar complementary force interaction within the actin and microtubule elements of their cytoskeleton (106).

The effects of the anticytoskeletal drugs were quantitatively inconsistent. The apparent tension in the actin network (the tension measured in the presence of nocodazole) was greater than the sum of the apparent compression in the MTs (measured in the presence of cytochalasin) and the compression of the dish (the rest



tension). The explanation we favor is that the surface interactions between actin and MTs (47,94) provide a stabilization, ie. a surface compression, whose magnitude is the difference observed above. Such an effect was expected and a formal model for the tension and compression relationships within the cytoskeleton includes a term for this force (17). An alternative explanation that we cannot rule out at present is that depolymerizing MTs causes a net increase in tension generated by the actin network.

The observed complementary force interaction between a surrounding tensile network and an internal compressive support, similar to the "tensegrity" architecture of Buckminster Fuller (34), has also been proposed by Ingber and others to explain cell shape (49,50). Tension in such architectures has the counter-intuitive effect of stabilizing elongated forms such as masts (34). Axons resemble tensegrity structures (34) in their very large ratio of length to cross-sectional area, their elasticity and strength, and the finding that the putatively tensile actin network is continuous beneath the plasma membrane while the compressive microtubules are arrayed as discrete, internal fascicles (47,94).

CHAPTER 2. Tension, Viscoelasticity and Growth
 in PC-12 Neurites.

INTRODUCTION

The cytoskeleton is widely thought to provide the mechanical basis for cell shape (2) in general and for neuronal cell shape in particular (60). Neurons are good systems for studying animal cell architecture because their exaggerated anisotropy facilitates quantitative mechanical measurement (30). In addition, the growth processes underlying axonal elongation are thought to reflect general dynamic processes determining cell shape (108).

External force has been shown to affect cell shape, polarity, and motility. Specifically, the role of tension in axonal elongation has long been recognized (112). More recently, Bray has demonstrated that tension alone is sufficient to cause axonal elongation (11). Under special conditions, Campenot observed cell body migrations that suggested both tension induced neurite growth and tension induced retraction that appeared to be very much the reverse of growth (20). For these reasons, we are interested in further investigating the role of tension in the control of neurite length.

Previous studies by our lab, using force calibrated glass needles to make short duration (1-2 sec) distensions on PC-12 neurites, indicated an Hookian elastic response to



tension (30). We also reported preliminary observations that longer duration distensions elicited an additional viscoelastic mechanical response. Clearly, to further our understanding of the role of force in determining neurite length, we need to characterize and distinguish these passive mechanical responses from active growth and retraction. Toward this goal, the present study will quantitatively investigate neurite mechanical response to long duration distensions.



MATERIALS AND METHODS

PC-12 cells were cultured as previously described (30,53). Neurite rest tensions and spring constants were measured by short duration distensions as described (30). Using a modification of this method, the neurite was subsequently exposed to a long duration distension (see figure 10). Specifically, an initial rapid micro-manipulation of the force needle orthogonal to the neurite center was followed by periods of 25 to 85 minutes during which the micromanipulator was undisturbed to observe neurite response. A trial was ended by lifting the force-needle and thereby releasing the neurite. From the video record of this distension, neurite axial tensions and distended lengths were determined as a function of time using the trigonometric method previously described (30). Measurements of orthogonal neurite distension (b) and corresponding needle deflection from equilibrium (d) were taken at intervals of 1-2 minutes. In some experiments, a stock solution of taxol in DMSO (gift of Dr. Mathew Suffness, Developmental Therapeutics Program of the National Cancer Institute) was added to the culture media to achieve a final concentration of 1 μ M taxol and 0.1% DMSO. Long duration distensions were begun 5-10 minutes after addition of the drug.



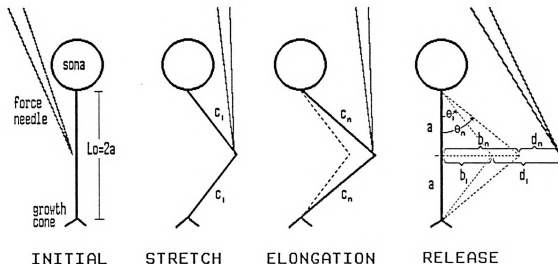
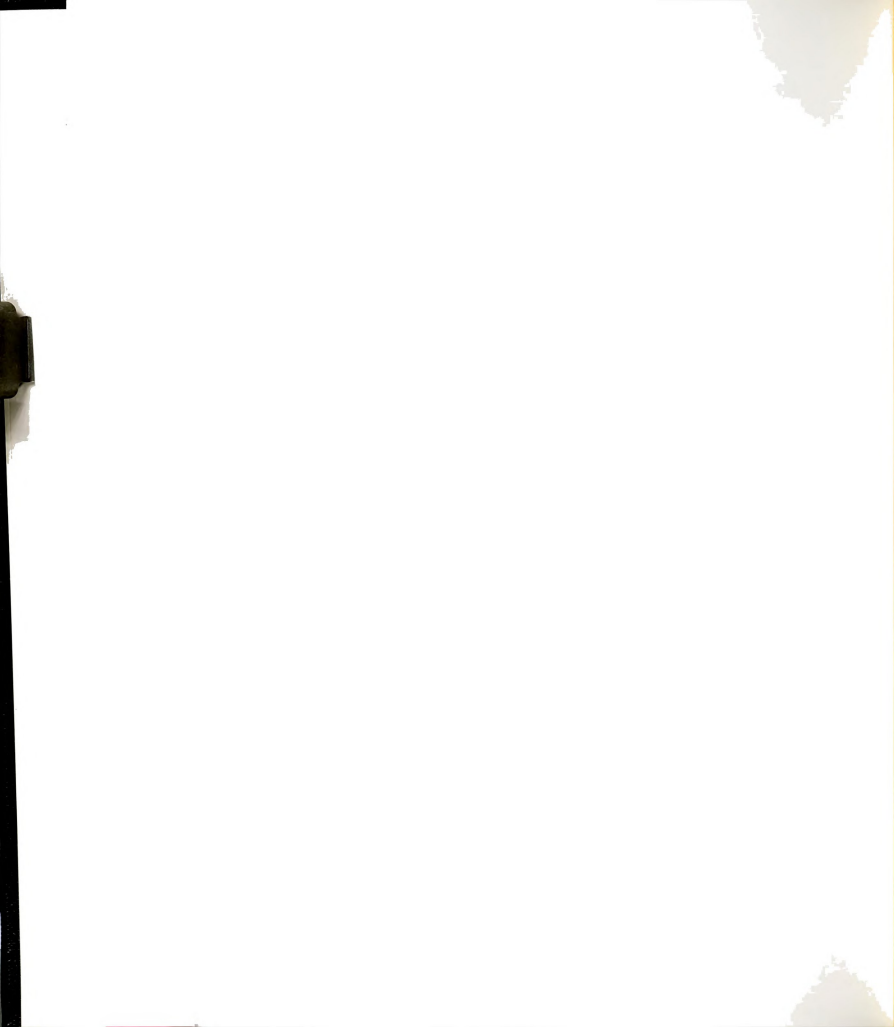


Figure 10. Method of measurement of PC-12 neurite tension during viscoelastic distension.

A force calibrated glass needle is initially placed at the neurite center and then deflected in an orthogonal direction causing an initial elastic stretch. Over time, the neurite elongates further. An experiment is ended by lifting the needle and releasing the neurite. After the experiment, measurements are made from recorded video images of neurite rest length (L_0), and at intervals of 1-2 minutes of neurite lateral displacements ($b_1, b_2 \dots b_n$) and force calibrated needle deflections ($d_1, d_2 \dots d_n$). These values are used to determine neurite axial tensions and lengths as a function of time.



RESULTS

Viscoelastic Response to Neurite Distension

In 20 trials on 13 PC-12 cells, neurites were continuously distended in a direction orthogonal to the neurite axis for periods of 25-85 minutes (see figure 10 and Materials and Methods). For eight trials initial applied forces were 100 udynes or less; under these conditions we observed a 2-phase viscoelastic lengthening response (see figure 11). Initially, there was a rapid increase in neurite length and tension (phase 1), followed by a slow damped increase in length and decrease in tension to plateau values (phase 2). Due to the dependence of force-needle deflection on neurite length following the initial micromanipulation of the needle, plots of neurite tension over time are mirror the plots of neurite length (see figure 11).

Recovery from such distensions following release was rapid; the neurite typically became visibly straight and normal in appearance within 1 minute. In all 8 trials, a series of short duration distensions were made 1 to 5 minutes before and 1 to 10 minutes after a long duration distension to determine if it had an effect on the neurite's elastic properties. Following long duration distensions, rest tensions averaged 108% and spring constants averaged 147% of initial values.

These data indicate that PC-12 neurites respond to low

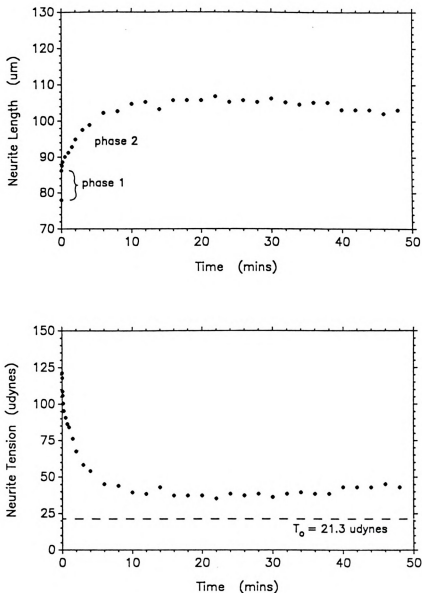


Figure 11. Tension induced 2-phase neurite elongation.

Resulting neurite length (above) and tension (below) is plotted as a function of time for an initial applied force of 99.7 udynes. Typical for applied tensions of 100 udynes or less, an initial elastic stretch (phase 1) is followed by a damped viscous elongation to a plateau (phase 2).

force, long duration distension as visco-elastic solids. By this we mean that the deformation response of neurites to applied force has both fluid-like and solid-like properties and at long time scales there is a final equilibrium between force and deformation as in a solid. We have modelled this behavior with a combination of 3 classical mechanical elements (see figure 12): a relatively stiff spring (spring constant k_1) in series with a Voight element consisting of a less stiff spring (k_2) in parallel with a dashpot (viscosity constant H). Values for these three mechanical constants were determined analytically (see Appendix A). As shown in figure 13, computer simulations of the expected behavior of our proposed mechanical model (see Appendix B) using the analytically determined spring and dashpot constants show a close match between expected and observed behavior in neurites of both PC-12 and chick sensory dorsal root ganglia. A deviation from theoretical tension values follows the first 10 minutes of distension in neurite 4; we interpret this deviation as a third phase of elongation (growth) as described below. It is impossible to fit all the data for this neurite by manipulating the three mechanical constants above. A more intuitive feel for the contribution of individual model elements is gained by simulating the behavior of a family of hypothetical neurites that vary only in one mechanical element; this is done in figure 14.

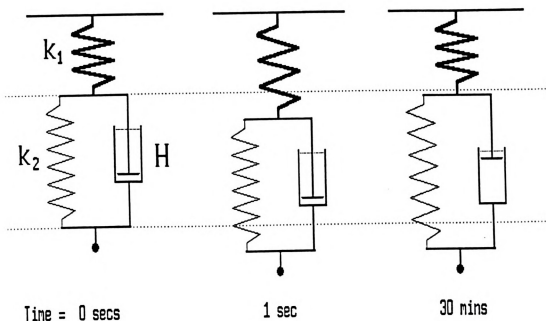


Figure 12. Viscoelastic model of neurite mechanical response to long duration distension.

We have modelled neurite viscoelastic behavior using classical mechanical elements as shown above. A relatively stiff "free" spring (spring constant k_1) is in series with a Voight element consisting of a second spring (k_2) in parallel with a dashpot (viscosity constant H). Pictured above is the behavior of such a system following an transient stretch which is then held stable. Initially, the system is at equilibrium at low tension (left). Immediately following distension (center), tension rises and is held completely by spring 1. Over time, the dashpot flows allowing spring 2 to elongate and hold more of the applied tension while spring 1 shortens as the total tension of the system declines. Finally, a new equilibrium is reached (right) at a longer length and at somewhat higher than initial tension. Changes in tension held by the system can be easily seen as relative changes in the length of spring 1.

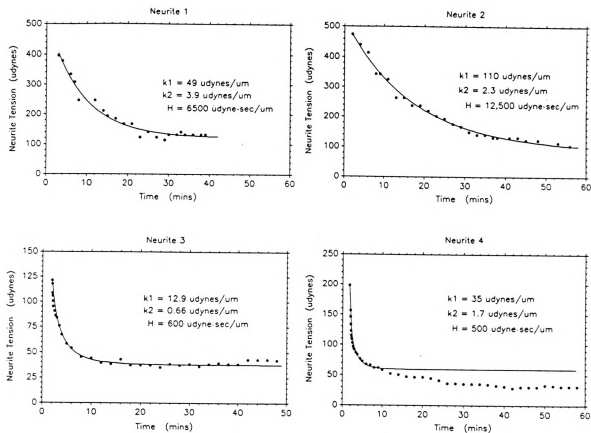


Figure 13. Computer simulation of observed neurite distensions using our viscoelastic model.

In each graph, individual points represent observed neurite tensions during a distension experiment. Reported values for spring constants k_1 and k_2 and dashpot viscosity constant H are empirically determined from length and tension changes over time as described in Appendix 1. The solid lines are theoretical tension values over time from a computer simulation of distension based on our viscoelastic model (see Appendix 2) using the reported mechanical constants. Plots for neurites 1 and 2 represent results from chick DRG sensory neurons (distension data courtesy of Phil Lamoureux). A two phase PC-12 distension is plotted for neurite 3 and a three phase PC-12 distension is plotted for neurite 4.



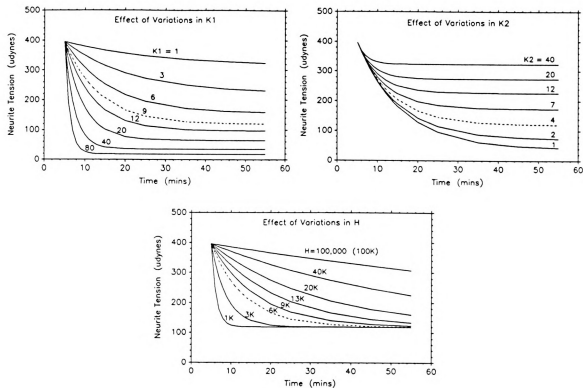


Figure 14. Computer simulation of hypothetical neurite distensions.

Hypothetical neurite tensions are plotted as a function of time where each plot shows the effect of varying the three mechanical constants (spring constants k_1 and k_2 , and dashpot viscosity constant H) independently. In all three plots, the single dashed curve represents a "standard" neurite with $k_1 = 9$ udynes/um, $k_2 = 4$ udynes/um and $H = 6000$ udyne*sec/um while the family of solid curves represent variations in the single labeled constant.

Tension Induced Phase 3 "Growth"

In 9 of the total 20 trials on PC-12 neurons, neurites were subjected to initial applied forces greater than 100 udynes and responded with an additional third fluid-like lengthening phase. By this we mean phase 1 and 2 proceeded as in the low force distension discussed above and was followed by a third period of elongation and tension decrease that either did not plateau during the experiment or plateaued only after neurite axial tension fell below a critical value of 50-100 udynes (see figure 15). In two cases, a neurite was exposed to both a low and high initial applied force; these are shown in figure 16. A clear qualitative difference between the low force (<100 udynes), 2-phase response and the high force (>100 udynes), 3-phase response is seen in both neurites.

Following release, neurites which had exhibited this 3 phase elongation typically lay flaccid and curvy on the dish for several minutes; the result of experimentally applied forces was an obvious elongation but no obvious thinning. Within 10-15 minutes, these neurites shortened and eventually tightened between the growth cone and cell body dish attachments. In 8 trials, when a series of short duration distensions were successfully made both before and after recovery from a long duration distension, final rest tensions averaged 42% and final spring constants averaged 84% of initial values.

For convenient analysis, we tentatively defined phase 3

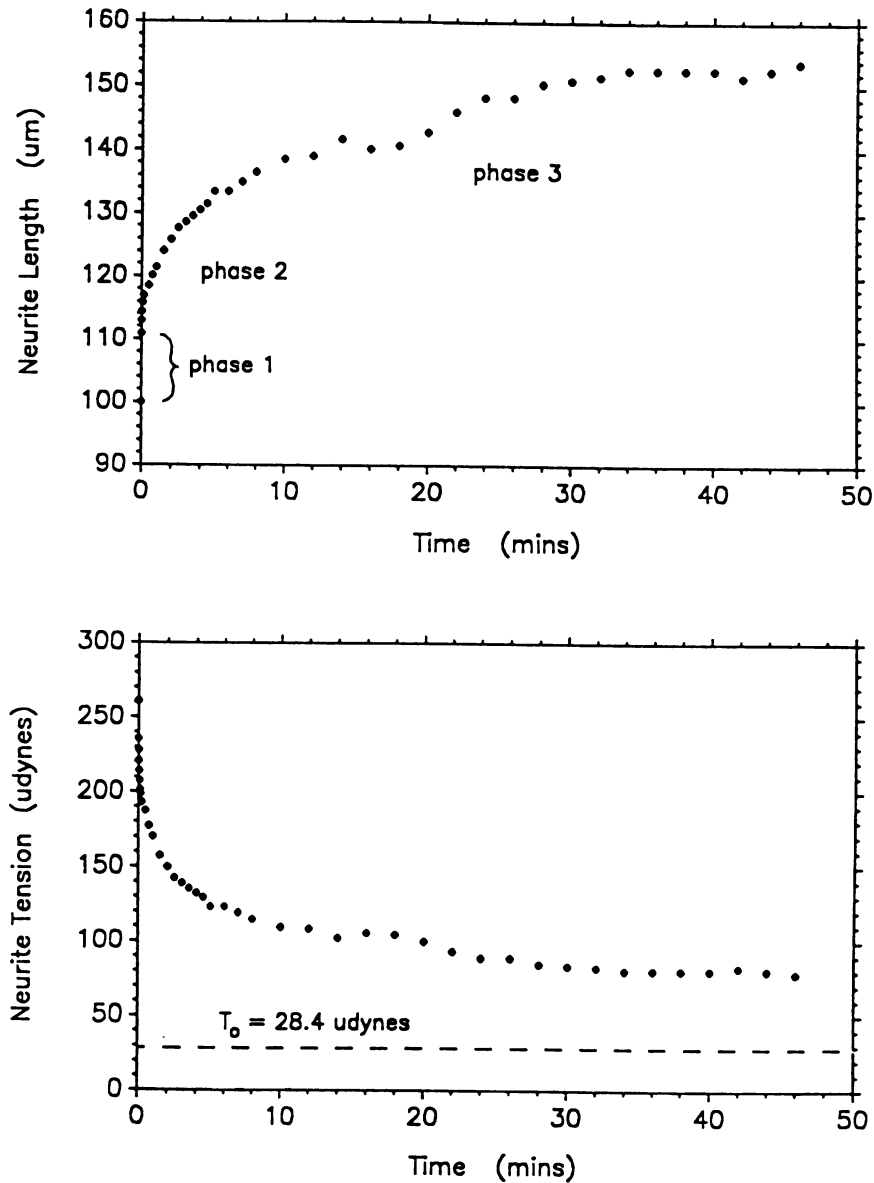
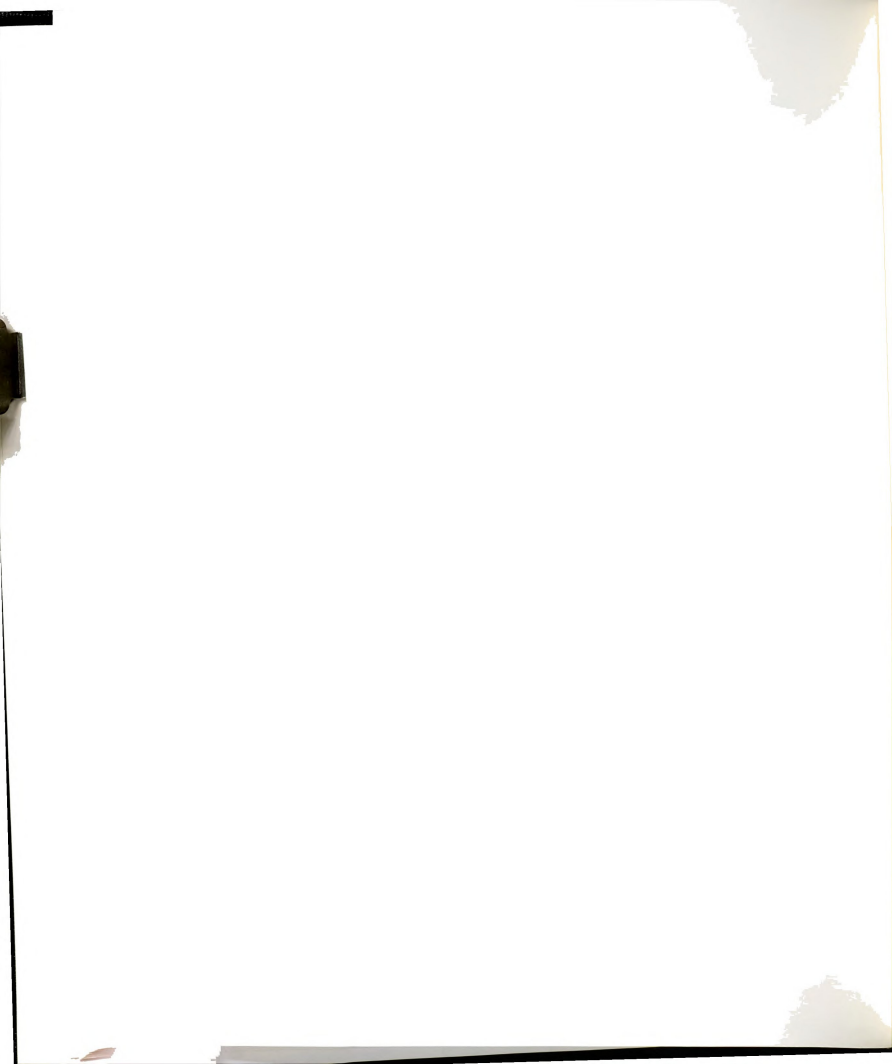


Figure 15. Tension induced 3-phase neurite elongation. Resulting change in neurite length (above) and tension (below) is plotted as a function of time for an initial applied force of 233 udynes. Typical for applied tensions of greater than 100 udynes, phase 1 and 2 elongation is followed by a viscous-like third phase of elongation.



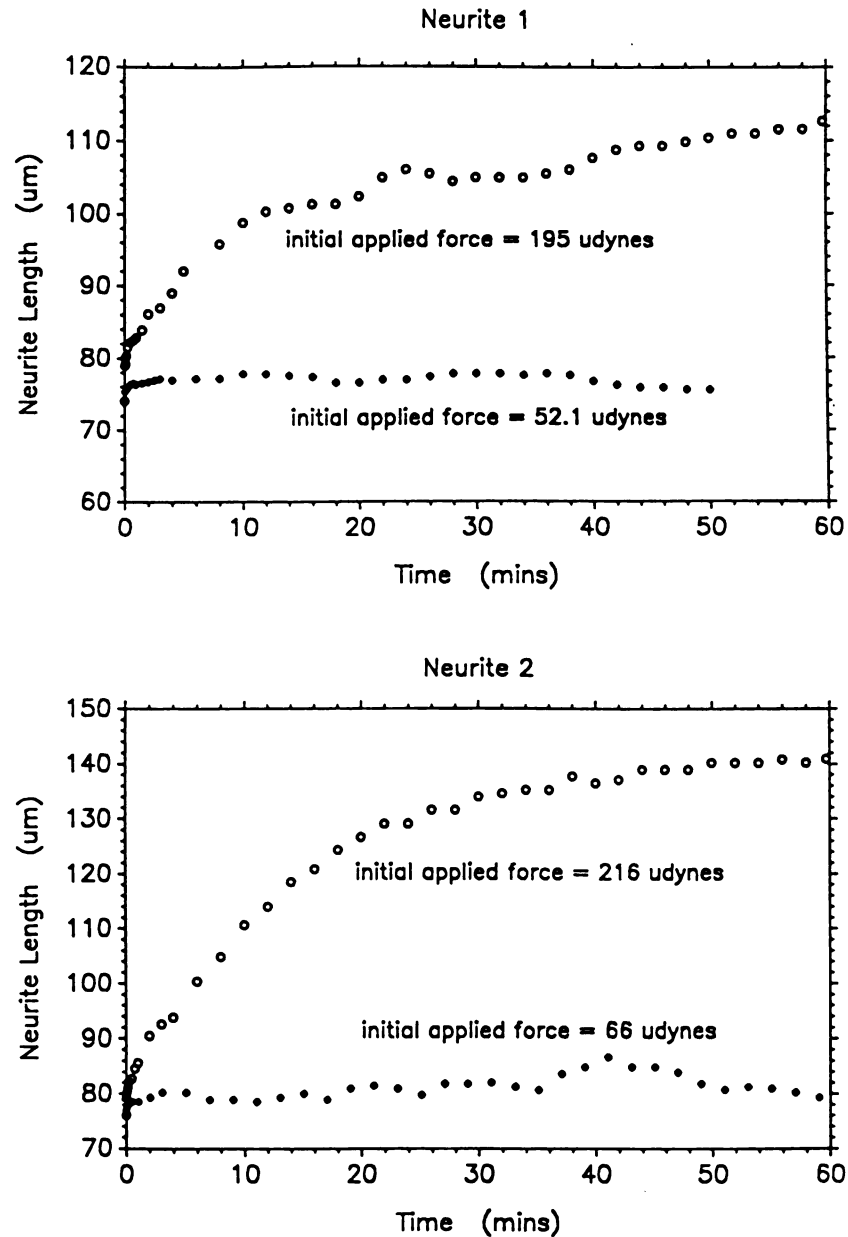


Figure 16. Low and high initially applied tensions on the same neurite.

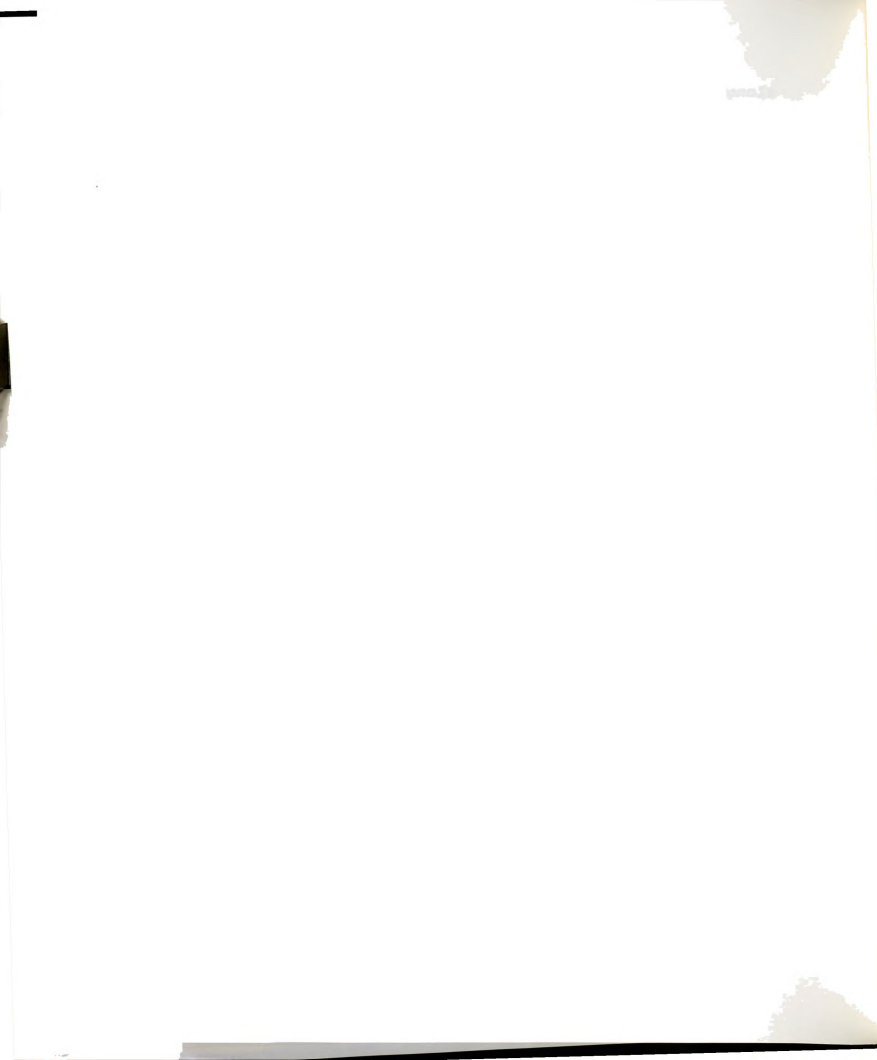
Plots of length change vs. time are shown above for two neurites that underwent both a low (<100 udynes) and high (>100 udynes) initial applied force.



elongation as beginning 10 minutes after the initial application of experimental tension. Figure 17 plots the resulting average rate of elongation during phase 3 against the initial amount of applied force for all 20 long duration distension trials. This plot shows a threshold value of approximately 100 udynes below which there is no positive phase 3 elongation rate, and a rough linear dependence of this elongation rate on applied force above 100 udynes. However in 3 of the total 20 trials on PC-12 neurons, the neurites responded to initial applied forces above 100 udynes by exhibiting a two phase lengthening response and rapid (< 1 minute) recovery typical of the response to initial applied forces below 100 udynes (see figure 17).

Taxol Inhibition of Phase 3 Elongation

In 5 trials on 5 PC-12 neurons, neurites were exposed to initial applied tensions above 100 udynes after the addition of 1 μ M taxol, a potent stimulator of microtubule assembly (91). In these neurites, phase 3 elongation is completely eliminated with little or no qualitative effect on either phase 1 or 2 (see figure 18). Experiments done in the presence of taxol exhibited fast recoveries following release from a high initial applied force; the neurite became visibly straight and appeared normal within 2 minutes of release of tension. In 3 out of 5 of these taxol trials, we were able to perform a series of short duration distensions both before and after the long duration



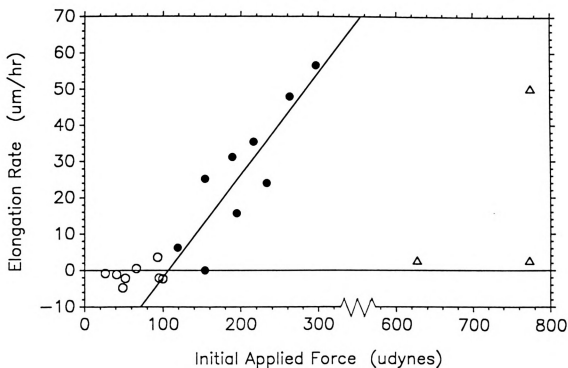
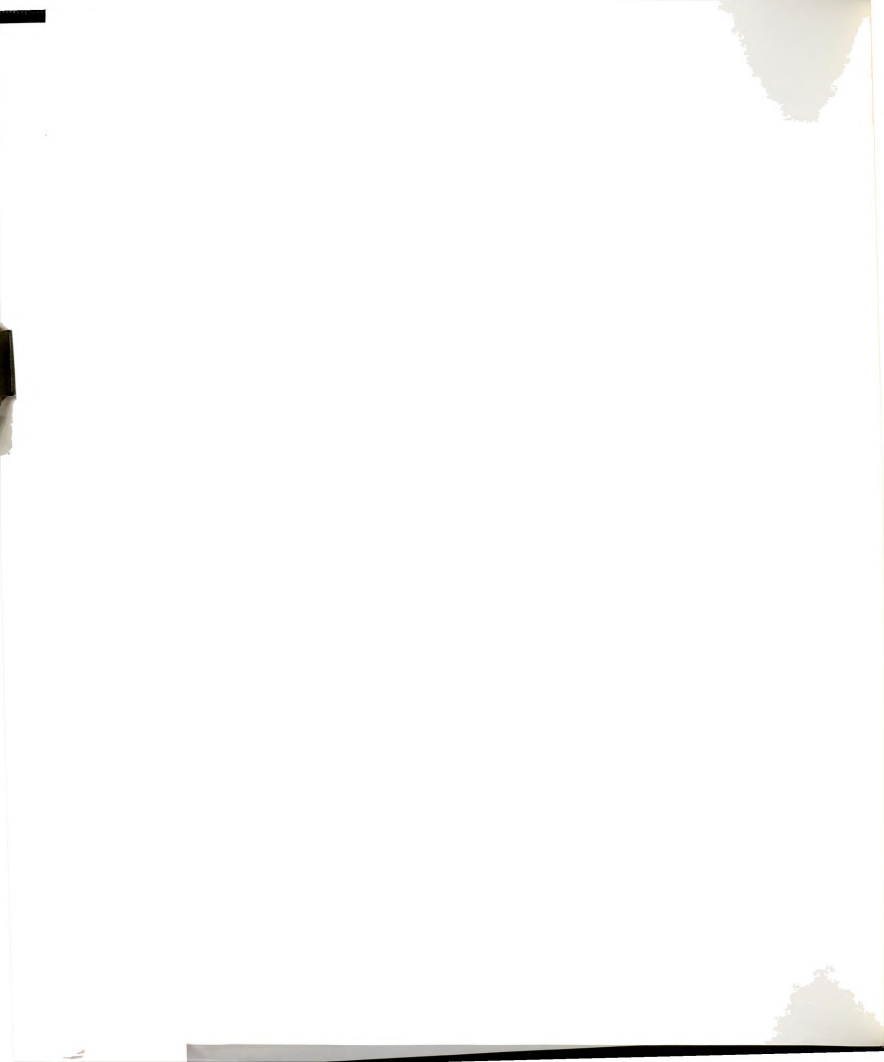


Figure 17. Threshold tension for phase 3 neurite elongation.

The average rate of elongation following the first ten minutes of distension (i.e. phase 3) is plotted against initial applied force. A least squares fit regression was done for all trials with initial applied forces between 100 and 300 udynes (filled circles) that gives a correlation of 0.871. All trials with initial applied force of 100 udynes or less (open circles) have near zero elongation rates. For unknown reasons, three very high initial applied tension trials (open triangles) exhibited non-typical behavior.



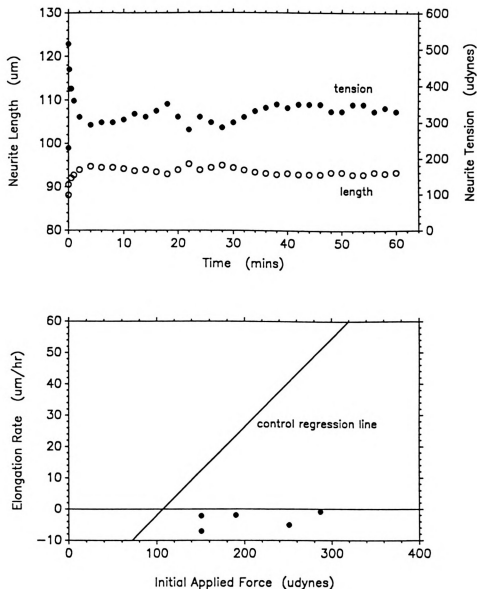
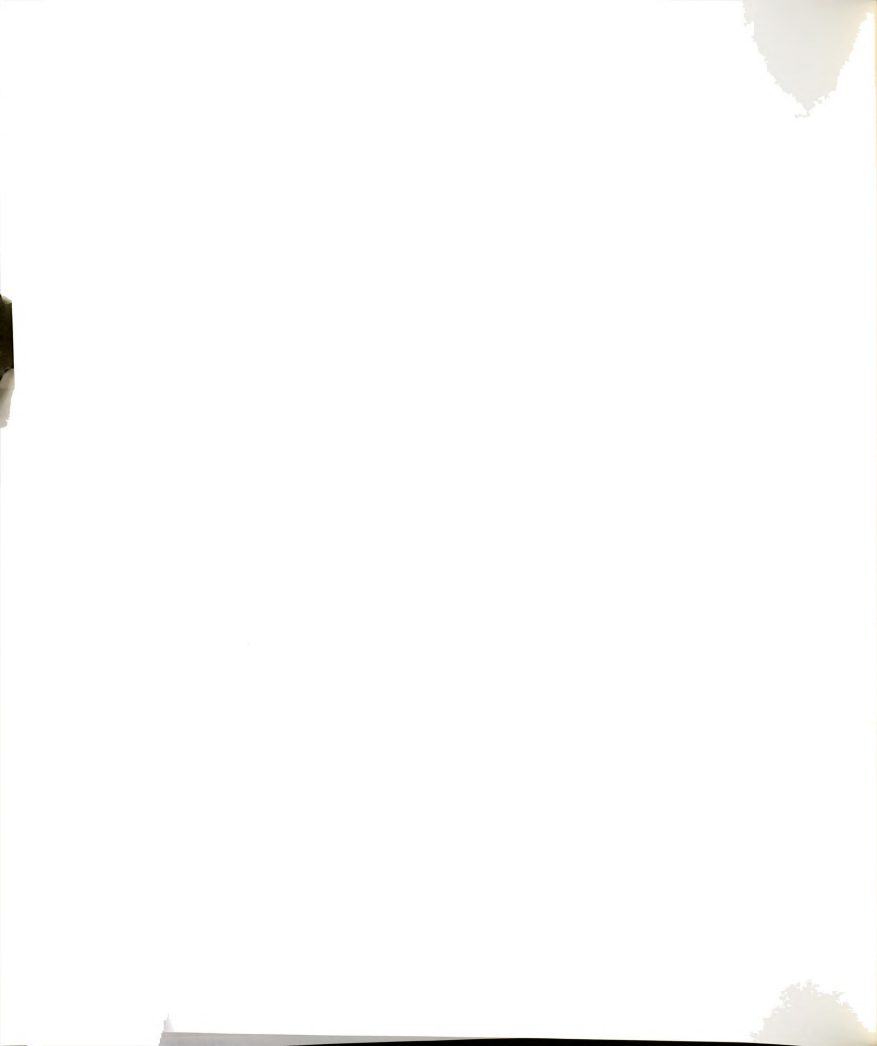


Figure 18. Taxol inhibition of phase 3 elongation.

Upper plot: resulting change in neurite length and tension in the presence of 1 μM Taxol is plotted as a function of time for a single trial with an initial applied force of 287 udynes. Lower plot: The average rate of elongation in the presence of 1 μM Taxol following the first ten minutes of distension (i.e., phase 3) is plotted against initial applied force for all 5 trials.



distension. In these cases, final rest tensions averaged 176% and final spring constants averaged 160% of initial values. These behaviors are distinct from five separate trials on five PC-12 neurons exposed to a series of short duration neurite distensions in the presence of 1 μ M Taxol. These experiments showed little or no effect on neurite tension or spring constants; rest tensions averaged 124% and spring constants averaged 95% of pre-treatment values.

1000
1000

DISCUSSION

We have found that PC-12 neurites behave as viscoelastic solids in response to long duration (25-85 minute) distensions at a low continuous applied force (figure 11). Specifically, these neurites respond with an initial elastic stretch (phase 1) followed by a damped viscous-like elongation that plateaus (phase 2). Recovery from these biphasic elongations is rapid, returning to original linear morphology within a minute following release. Rest tensions and spring constants (measureable in 1-10 minutes) also recover to near pre-distension values. Studies on sea urchin eggs (44,46,73) and lymphocytes (80) also indicate viscoelastic solid behavior when mechanical measurements are made on the intact cell.

We interpret the neurite's biphasic distension as a passive mechanical response to force and have modeled neurite viscoelastic behavior with a combination of three classical mechanical elements: two springs and a dashpot (figure 12). The free spring (k_1) is able to respond instantaneously to an applied load by lengthening in proportion to the load. The same elastic element appears responsible for both the spring constant measured in short duration distensions (30) and for the initial rapid elongation (phase 1) in long duration distensions. It appears that there is a Voight element in series with this free spring, ie. a second spring in parallel with a dashpot.



This Voight element also responds to force like a spring with a load proportional elongation, but does so in a delayed (damped) fashion due to the viscous drag of the dashpot. This pair of elements models the damped approach to plateau length and tension (phase 2) seen in long duration distensions. The validity of this mechanical model is strongly supported by the close match between experimentally observed responses to long duration distensions and computer simulations using analytically determined values for spring and dashpot constants for a particular neurite (figure 13 and Appendices A and B). Earlier work with cytochalasin D (30) points to a strong association of the polymerized actin network with the free spring (k_1). Unfortunately, most drug studies are too crude in effect to be of much value. Future studies in our lab are aimed at developing more specific perturbations of cytoskeletal elements to better define functional roles of individual structures in the cell for each of these measurable mechanical constants.

PC-12 neurites exposed to initial applied forces of greater than 100 udynes showed an additional third phase of elongation at a constant rate (figure 15) which we will interpret as "towed" neurite growth similar to that seen by Bray in response to experimentally applied tension (11). This interpretation is supported by the observation that neurite lengths increased up to 218% of initial length during distension, with no observable changes in diameter

and no obvious structural damage. These neurites recover their original morphology after release, but rather slower than neurites exhibiting a two phase elongation response. This putative towed growth appears to occur above a tension set point of approximately 100 udynes. Above this tension load, towed growth occurred in 8 out of 12 neurites with a roughly linear dependence of growth rate on applied force (figure 17). Below this level, all 8 neurites showed near zero elongation rates. The existence of a set point is further supported by the different elongation behavior of two neurites that experienced initial applied forces below and above 100 udynes (figure 16). We investigated the role of microtubule assembly in phase 3 elongation by observing the effects of 1 μ M taxol, a known stimulator of microtubule assembly (91). In long duration distensions with an initial applied force above 100 udynes, taxol treatment showed no effect on phase 1 or 2 elongation, but the phase 3 elongation rate was strongly inhibited. This result suggests that tension induced (phase 3) growth is dependent upon microtubule assembly. Taxol may be disrupting the normal microtubule assembly necessary for neurite growth in a manner similar to the observed taxol inhibition of normal neurite growth, as reported by Letourneau and Ressler (64). This could be the result of tubulin dimer depletion, or of a structural interference in the growth process caused by the addition of the "taxol microtubules".

Others in our lab have shown that the neurites of chick



sensory dorsal root ganglion neurons also respond viscoelastically to externally applied force (figure 13). In addition, they are able to actively generate tension in response to decreases in applied force (41). When these neurites are slackened, they respond with a biphasic shortening and tension recovery that looks like the inverse of the 2-phase length and tension response to distension discussed above for PC-12. Significantly, in greater than 60% of these experimental trials, tension recovery exceeded (and sometimes even doubled) initial pre-slackened values. This behavior clearly suggests active tension generation by the neurite shaft. A historically interesting parallel here is that some 60 years ago muscle was still being described as a "viscous-elastic system" capable of exerting force by shortening (66).

The story emerging from our data is that neurite (or axon) length is sensitive to a continuum of axial tension. At tensions above a particular value, the neurite grows in length; at intermediate tensions it responds as a viscoelastic solid; and when neurite tension falls below a particular value the neurite shaft is stimulated to generate tension and retract. These results suggest a 3-position controller for neurite length response to changes in axial tension (figure 19). The postulated 3-position controller is distinct from one where the neurite may be responding to changes in axial tension with a purely proportional response. A proportional response occurs when there are no



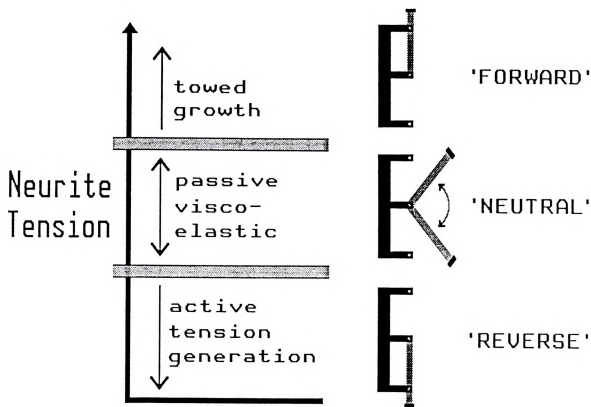


Figure 19. 3-position controller model for tension dependence of neurite length.

The figure at left summarizes the three observed tension-dependent neurite behaviors and the cartoons on the right depict a hypothetical 3-position controller analogous to a 'Frankenstein-type' switch that would be used to control an electric motor. This switch represents a tension-sensitive controller that is able to initiate either neurite assembly (towed growth) above an upper tension threshold or neurite contraction (active tension generation) and/or disassembly below a lower tension threshold. At intermediate tensions, the switch is not activated and the neurite behaves passively as a viscoelastic solid.

set points, just a continuum of response from shortening to lengthening as tension increases. It is possible that growth is proportionately controlled and that PC-12 neurites that have zero growth rates in response to applied tension (figure 17) were in a refractory mode and insensitive to force stimuli. This seems unlikely because it would imply that neurites at their "natural" rest tension (zero applied force) are all either in the process of shortening or are refractory. To the contrary (and as logic dictates), we observed undisturbed PC-12 neurites in culture to have a positive elongation rate averaging 5.3 $\mu\text{m/hr}$ (30).

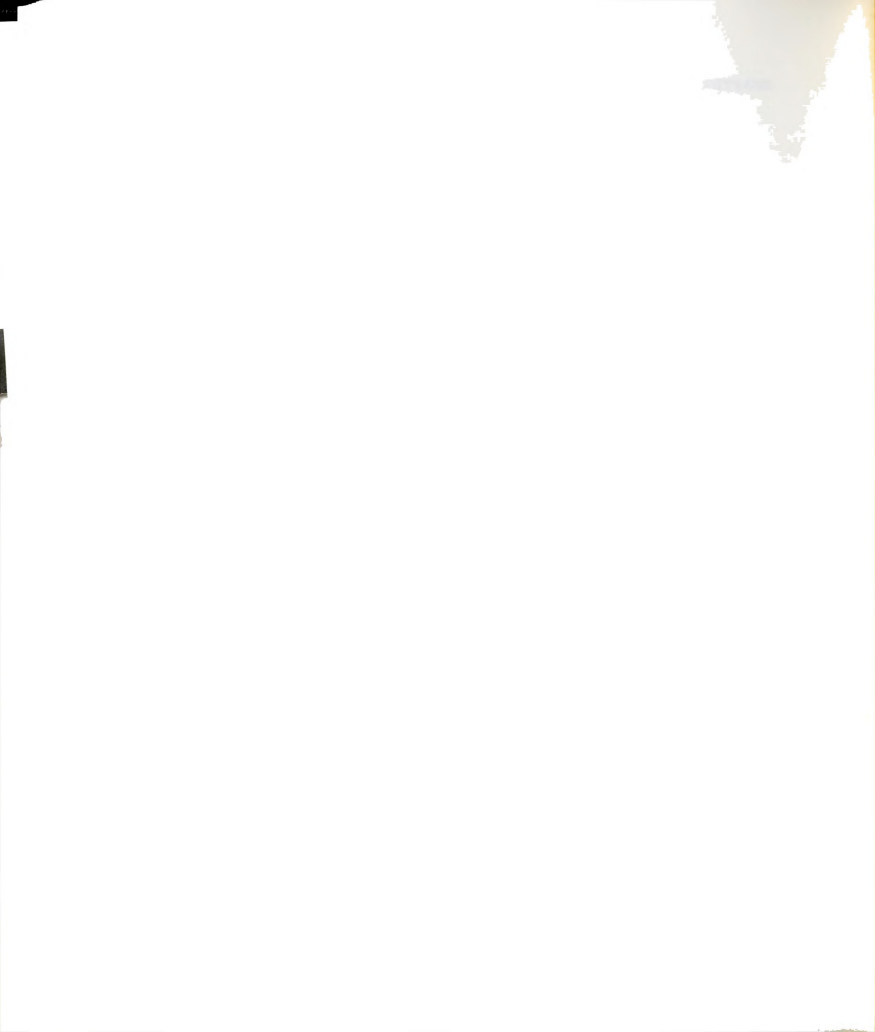
The tension dependence of neurite length control is significant for several reasons. Tension has been long inferred to be responsible for the passive axonal elongation during growth to adult body size that must follow embryonic synapse formation (112). Bray elegantly demonstrated that tension is sufficient for axonal growth (11). In addition, recent work by our lab indicates that the growth cone is indeed a pulling motor (59). Together these results suggest that tension may be the cause of axonal elongation generally. Mitchison and Kirschner (74) have pointed out that tension is an attractive "second messenger" for growth control based on a priori arguments. This behavior is also consistent with our thermodynamic model for the regulation of microtubule assembly by force (59). In this model, the advancing growth cone transfers tension support (compression) from the internal microtubule core onto the

underlying substrate. This results in both a net increase in neurite tension and a decrease in microtubule compression, decreasing the critical concentration of tubulin dimer for assembly. Assuming equilibrium conditions prior to growth cone advance, net microtubule assembly and neurite elongation occur until equilibrium is restored. Similarly, a loss of growth cone adhesion would increase microtubule compression and cause disassembly and neurite shortening. We have observed such a compression induced disassembly of microtubules in PC-12 cells by releasing neurite adhesion with surface active agents and measuring changes in the soluble:polymerized tubulin ratio with quantitative immunoblotting (30).

CHAPTER 3. F-Actin and Microtubule Suspensions as
Indeterminate Fluids.

INTRODUCTION

Actin and Microtubules are among the most widely conserved structural proteins within eucaryotic cells. It has been long suspected that the viscoelastic properties of these polymers (particularly F-actin) play an important role in the maintenance and development of cell shape and in cellular motility (82,102,105). Mauryama et al. (71) found that the measured viscosity of F-actin was precisely inversely proportional to the shear rate. These workers reported on the uniqueness of this inverse proportionality and speculated that it may be the result of the formation of an actin network. Subsequent rheological studies confirmed that F-actin suspensions are shear thinning but did not find the same shear-viscosity dependence or did not discuss this relationship (87,88,120). We confirm the observation of Maruyama et al. for actin and observe a similar inverse proportionality for suspensions of microtubules. Also, we show that as a result of this dependence, the fluid flow profiles for such suspensions are indeterminate. That is, a given force does not fix the velocity of movement in these fluids.



MATERIALS AND METHODS

Actin was purified from rabbit skeletal muscle by the method of Spudich and Watt, or by their method and further purification by chromatography on Sephacryl S-200 (Pharmacia, Piscataway, NJ) (68,101). Purified actin was maintained in dialysis at 4°C against buffer A [2.0mM tris-HCl, pH8.0, 0.2 mM ATP (adenosine triphosphate), 0.5 mM mercaptoethanol, and 0.2 mM CaCl₂] for no more than 6 days. Microtubule protein was purified from beef brain in the presence of glycerol according to the method of Shelanski et al. (97) with the modification that 0.1 M PIPES (piperazine ethanesulfonic acid), pH 6.6, was used in all reassembly buffers. A model R.18 modified (72) Weisenberg cone and plate rheogoniometer was used for all rheometry experiments. Actin was polymerized by adding KCl to a final concentration of 50mM and MgSO₄ to a final concentration of 2 mM to G actin at various concentrations in buffer A. The mixture was applied quickly to the bottom cone (2°, 5 cm in diameter) of the rheogoniometer, the upper plate was immediately lowered to the correct height above the cone, and the actin was polymerized for 1 hour at 23°C before measurements were made. Microtubule protein suspended in 0.1 M PIPES, pH 6.9, 1 mM MgCl₂, 1 mM EGTA, 0.1 mM EDTA, and 0.5M GTP (guanosine triphosphate) was polymerized at 37°C for 20 minutes and applied to the cone of the rheogoniometer. A humidified atmosphere was maintained



around the cone and plate assembly by adding a small pool of water to the floor of the instrument's temperature control chamber. For each sample of protein loaded into the rheometer, 10 to 14 shear rates (drive settings) were chosen to obtain torque readings. After each torque reading the drive was turned off and the torque allowed to return to baseline before we reset the drive for the next reading. Measurements on a single protein sample took approximately 2 hours. The rheogoniometer was calibrated with a Newtonian viscosity standard (R12000, Cannon Instrument Company). Values for viscosity and shear rate were calculated from rheogoniometer drive settings and instrument readings by standard formulas. Polarization micrographs were taken with a Leitz Ortholux I Pol microscope, at 1200x.

RESULTS AND DISCUSSION

Figure 20 is a Logarithmic plot of viscosity versus shear rate for two runs of actin at different concentrations, two runs of microtubules with and without taxol [a stimulator of microtubule assembly (91)], and one run of the viscosity standard. The values reported in Fig. 20 and throughout this report are the stable values obtained after shearing the fluids for several seconds. As found previously for actin (71) in both actin and microtubule suspensions, the torque rises sharply as shear begins but then declines to a stable value over a time period that depends on the shear rate. In addition to the shear-thinning behavior characteristic of all polymer suspensions, these plots show that the power law dependency for actin and microtubule suspensions is nearly -1 for all concentrations. That is, actin and microtubule suspensions behave as power law fluids with

$$V = A(ds/dt)^n \quad (\text{Eq. 1})$$

where V = viscosity, A is a constant, ds/dt is shear rate, and n is the power law exponent. In 12 runs of actin at concentrations from 2 to 6 mg/ml the exponent varied from -0.85 \pm 0.02 (\pm standard error of the regression coefficient) to -1.15 \pm 0.01 with a mean of -1.00. Both extreme values occurred for actin at 2 mg/ml, a

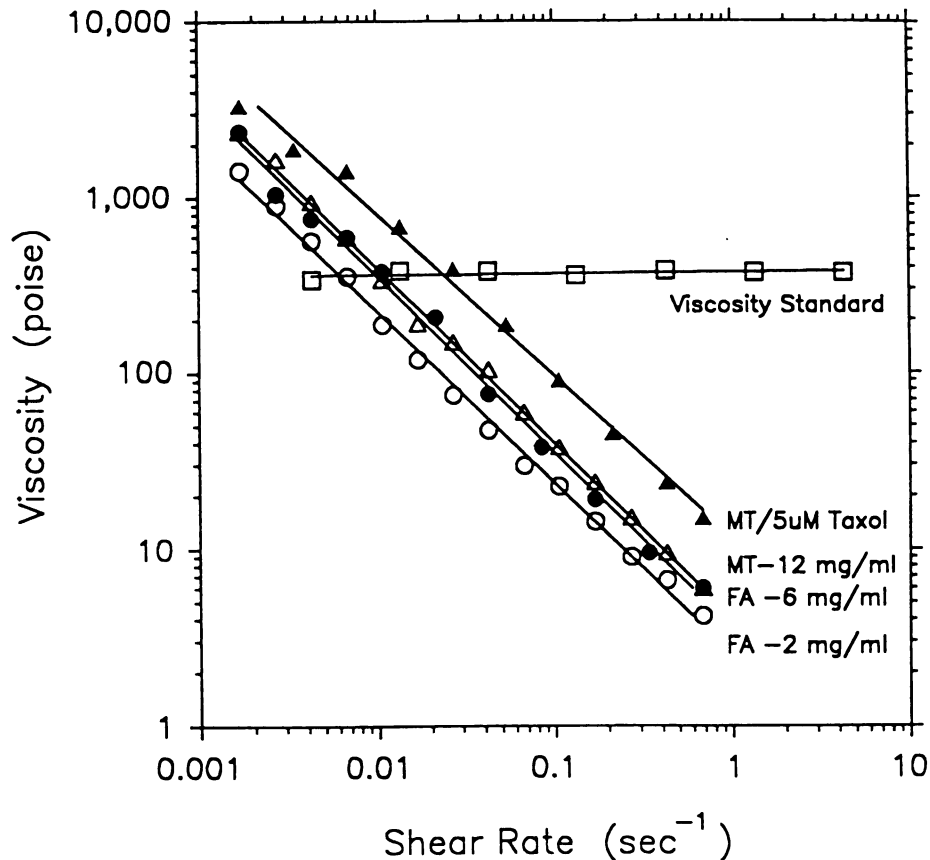


Figure 20. Viscosity as a function of shear rate for F-actin and microtubule suspensions.

Viscosity measurements at various shear rates on suspensions of cytoskeletal proteins and a viscosity standard at 23°C are shown on a log-log plot. (●) F-actin, 6 mg/ml, slope = -1.00 ± 0.02 ; (○) chromatographed F-actin, 2 mg/ml, slope = -0.98 ± 0.02 ; (Δ) polymerized microtubule protein, 12 mg/ml, slope = -1.00 ± 0.01 ; (▲) microtubule protein 12 mg/ml, polymerized in the presence of 5 μ M taxol, slope = -0.95 ± 0.3 ; (□) R12000 viscosity standard, slope = 0.00 ± 0.01 .



concentration that produces a torque on the rheogoniometer at its lower limit of resolution. In seven microtubule runs the exponent varied from -0.90 ± 0.01 to -1.03 ± 0.03 with a mean of -0.94 . The -1 slope (on log-log plots) was found to be nearly independent of the shearing history of the sample, as shown in Fig. 21. The slope of the line for increasing shear (-1.00 ± 0.02) is nearly identical to that for decreasing shear (-1.01 ± 0.02). In a run of chromatographed actin (3 mg/ml) in which the shear rate was varied at random the power law dependence was -0.99 ± 0.09 . The power law dependence of the microtubule suspensions viscosity was similarly insensitive to shear history. Our measurements varied only slightly. The small standard errors of regression coefficients indicate little variation of points around the calculated line. The slope from run to run also varied little at nominally the same conditions. In five runs of actin at 6 mg/ml from three different actin preparations the mean slope was 1.01 ± 0.04 (SEM). The possibility that our results are due to slipping at rheometer surfaces is eliminated by the finding that actin and microtubule suspensions pour easily and are well mixed after the shearing process in the rheometer. The observed viscosities for suspensions of these two filamentous constituents of the cytoplasm are consistent with previous in vivo measurements of cytoplasmic viscosity. Figure 22 shows a comparison of data obtained from various cytoplasmic studies with those obtained from an F-actin

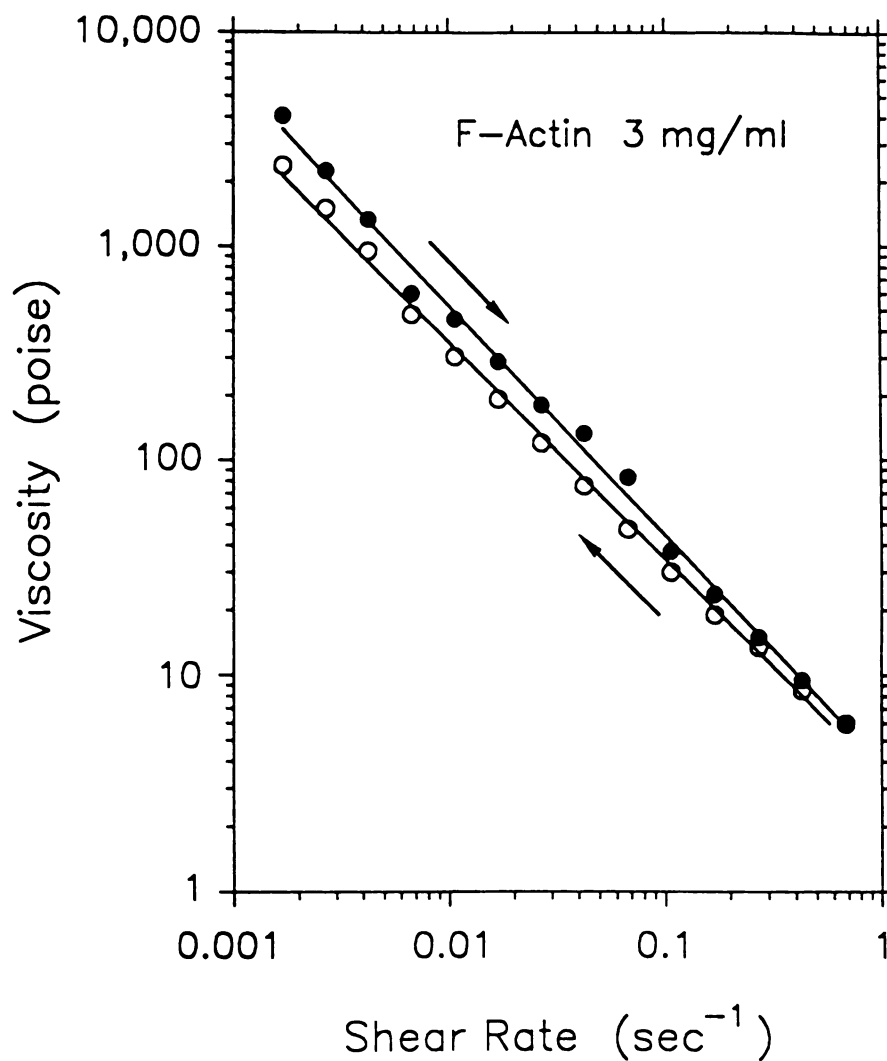


Figure 21. Effect of shear history on viscosity of F-actin. Two shear protocols for chromatographed F-actin, 3 mg/ml, from low to high rates of shear (\bullet), slope = -1.00 ± 0.02 and from high to low rates of shear (\circ), slope = -1.01 ± 0.02 .



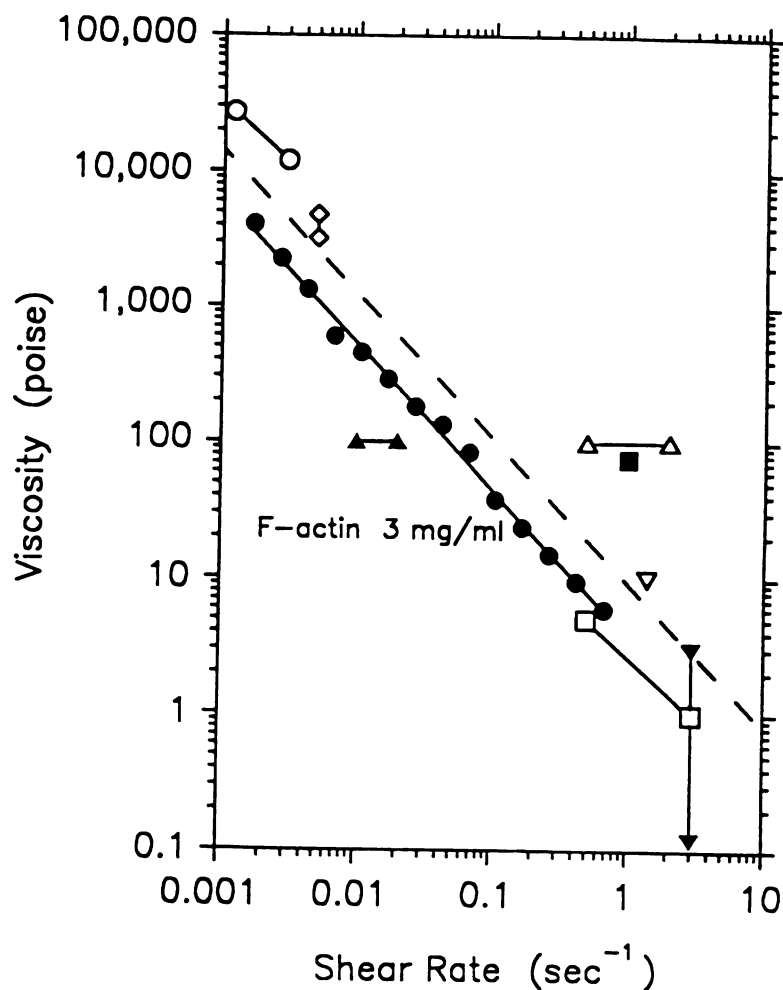
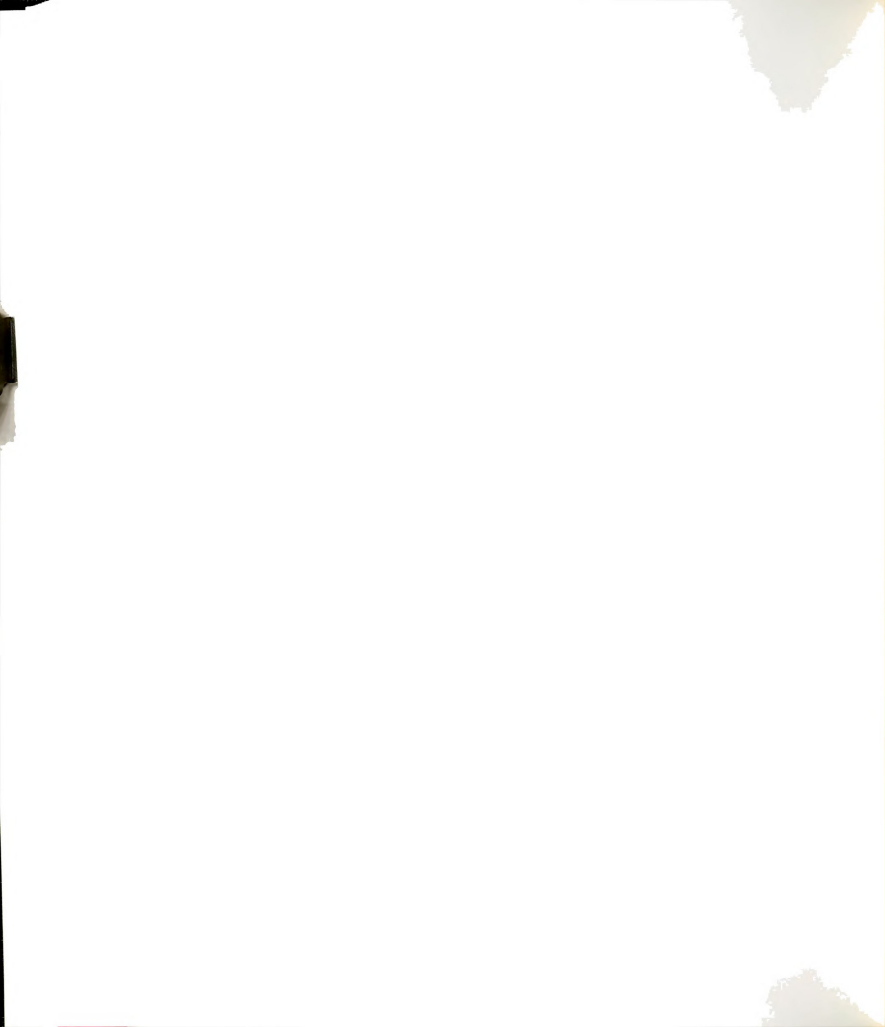


Figure 22. Viscosity of F-actin compared with viscosity measurements of cytoplasm by various in-vivo methods.

(●) F-actin, 3 mg/ml; (○) pulmonary macrophages, Valberg and Albertini (109); (◇) particles in lungs, Nemoto (77); (▲) human neutrophils, Sung et al. (103); (△) sea urchin egg, Hiramoto (45); (■) airway mucus, King and Macklem (56); (□) physarium, Sato et al. (90); (▽) chick fibroblasts, Crick and Hughs (26); (▼) amoeba, Yagi (116). The linear regression for the in-vivo data (---) gives a slope of -1.02 ± 0.18 .



suspension at 3 mg/ml. This similarity of viscosity function in vitro and in vivo is particularly interesting in view of the lack of true cross-links within purified F-actin (119) and the highly cross-linked nature of the cytoplasm (43,93,115). Power law observations in this range are significant because they contradict Graessley's classic random-coil-entanglement explanation that suggests the minimum n value is $-9/11$ (37,38). Typically, data show n between -0.4 and -0.85 for polymer solutions (7). Significantly, since shear stress is viscosity multiplied by shear rate

$$T = V(ds/dt) = A(ds/dt)^n(ds/dt) = A(ds/dt)^{(n+1)} \quad (\text{Eq. 2})$$

where T is the shear stress (force per unit area). Our observation that $n = -1$ means that shear stress is independent of shear rate. In this case, fluid motion is completely indeterminate. In Fig. 23 we plot shear stress data for actin, microtubules, and the Newtonian fluid standard. One's intuition, for example, on the basis of flooded rivers, is that increased shear rate increases shear stress. As shown in Fig. 23, the Newtonian standard follows the intuitive expectation. However, for both actin and microtubules the shear stress remains constant at all shear rates tested. This constant is the value A in equations 1 and 2.

In these experiments we controlled the shear rate and



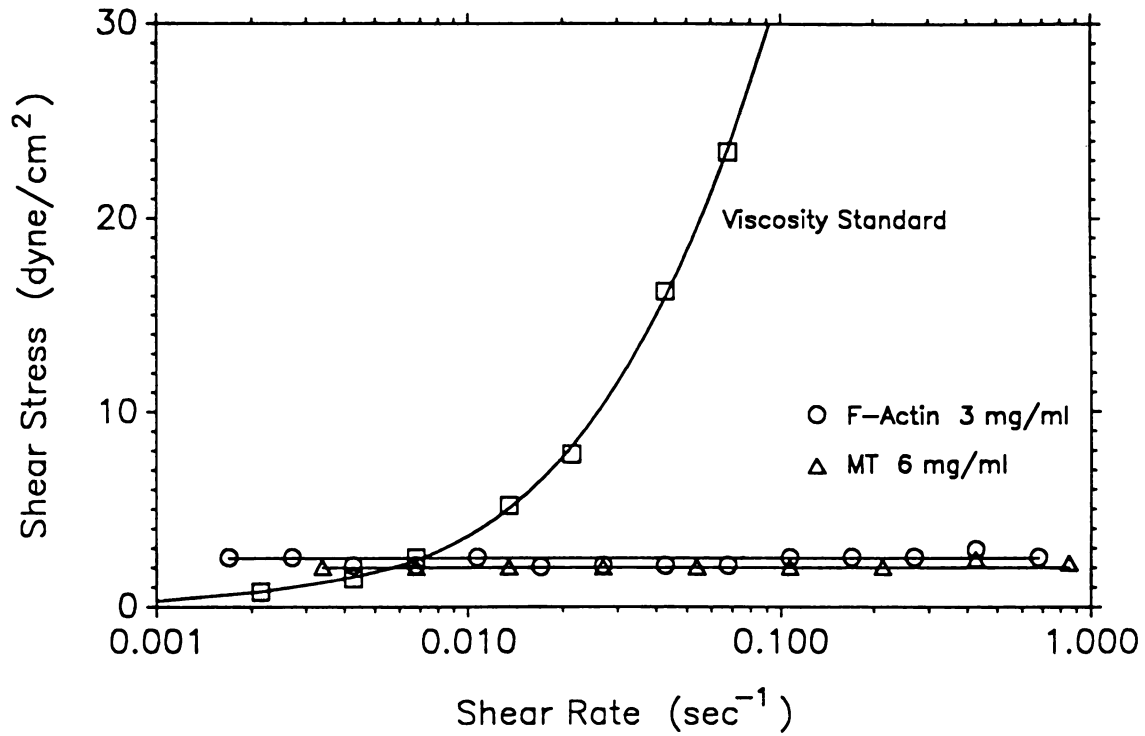
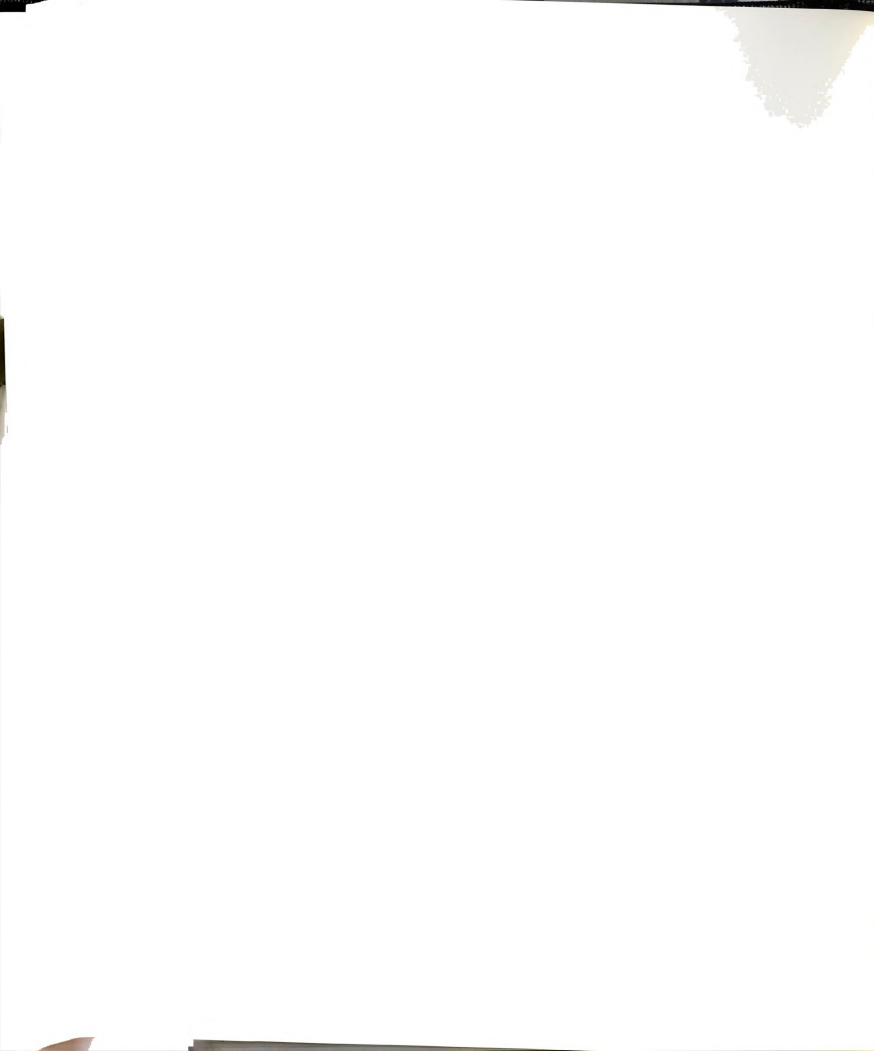


Figure 23. Shear stress as a function of shear rate for cytoskeletal proteins and the viscosity standard.
 (○) F-actin, 3 mg/ml; (△) polymerized tubulin, 6 mg/ml; (□) R12000 viscosity standard.



measured the force. In most biological (and other) situations, however, the interaction is reversed: a pump, a gravitational potential, or a cell supplies a particular shear stress, and the flow pattern accommodates it. However, as shown in Fig. 23, a force alone cannot fix the flow patterns for actin and microtubule (that is, indeterminate) suspensions. For any geometry, only one force pattern gives reasonable flow rates; push with less force and there is no motion, push with more force and the fluid velocity is limited by inertia alone.

Actin and microtubules are widely regarded as important in determining the physical properties of cytoplasm (82,102,105). Energy-dependent movement of particles through the cytoplasm occurs in all eucaryotic cells, and cytoplasm itself is capable of rapid, energy-dependent movement in some cells (54,86). Our data suggest that the velocity of movement is not limited by force, and the low Reynolds number characteristic of living systems suggests that inertia is not responsible. By deduction then, the observed velocities are fixed by the chemical kinetics of the biological motors. For example, structures within cells move suddenly over moderate (~ 30 μm) distances at constant velocity, and they halt equally suddenly (86). One explanation is that no motion occurs until a threshold force is reached, then a constant velocity is maintained by the stable kinetics of the mechanochemical motor.

The unusual field dynamics of nearly indeterminate



fluids may also explain the flow properties that characterize cytoplasmic streaming in various cells (54). In these cells, shearing flows are contained by cell membrane-cortex structures or, in the case of algae, by cytoplasmic walls. The flowing cytoplasm and the containing cytoplasm are fundamentally similar in their content of water and proteins. Flow indeterminacy may explain how these two regions of similar chemistry have such different velocities while bearing the same stresses. Possibly, the cell pushes the cytoplasm at constant force in some part of the cell and drags on the cytoplasm in the rest of the cell (necessarily with the same force per unit area). If the area pushing is smaller than the area dragging, there will be no cytoplasmic flow. If it is larger, flow is rapid. Thus for finite flows and equal shears on the cytoplasm and membrane, small differences in chemistry can produce enormous differences in flow.

This viscosity relation may also play a role in slow axonal transport, which involves a flow of cytoskeletal elements down the neural axon at a variety of different rates characteristic of the different cytoskeletal elements (48,113). If the fluid flow is nearly indeterminate and the axonal pressure drop will greatly affect their transport rate down the axon.

Another possibility from shear-thinning behavior that does not require flow indeterminacy concerns organisms that locomote upon a slime trail. In most instances this slime



is a polymer solution that would be shear thinning; most crawling results from sustained oscillations of contraction and expansion. Two models are possible: (i) an asymmetric oscillation in space so that the moving area is always smaller than the stationary area or (ii) an asymmetric oscillation in time both with the condition that the drag on the front of the organism over the substrate is determined by Newtonian viscosity (in water, for example) and the drag on the rear of the creature is determined by shear thinning slime. Then, as in Fig. 20, if the cell extends faster than it contracts, a net force will move the organism forward. Snail slime possesses "solid-like" properties at low shear rates (31) in concert with a shear-thinning fluid model.

The rheology of actin suspensions has generally been thought to be the result of network destruction by shearing (69,71,119). Although microtubule suspensions do not form gels or the looping entanglements required by the network theories (37,38,87,88), they have the rheological properties of actin suspensions. Further, the limiting power law exponent for entangled polymers is calculated to be $-9/11$ (37,38). Our data (Fig. 21) also indicate that shearing history has a relatively small effect on the viscosity of actin and microtubule suspensions. These observations suggest that network destruction is not primarily responsible for the rheology of these filamentous proteins. We have formulated two alternate models for these viscosity observations.

One model follows a suggestion of Zanner and Stossel (120) for actin suspensions and assumes that semidilute suspensions of rigid rods are at concentrations below the liquid crystal formation (that is, an isotropic distribution of the rods in space before shearing). In this model, as treated Doi and Edwards (32) and by Jain and Cohen (52), a large obstructional effect is caused by the constraint that rods cannot pass through each other. Assuming that the frequency of rod-rod obstructions is due to shear independent Brownian motion, Doi and Edwards (32) found regions where shear stress is independent of shear rate. To the extent that this model is appropriate, the phenomenon that is typically called "gelation" (true solidification) in the biological literature is seen as the "glass" (liquid with solid properties) transition induced by this obstructional constraint. This glass transition explains why the viscosity of cytoplasm and actin suspensions is so similar, that is, why crosslinkers in cytoplasm have so little effect on viscosity, as shown in Fig. 22. It also explains why actin "gels" behave as liquids. This "log jam model" can predict the observed -1 power law dependence of the viscosity and also that the power can be smaller than -1 over small ranges of shear.

We propose a second model to explain the observations with relatively flexible actin filaments and to extend the applicable concentrations above those for liquid crystal formation. This model differs from the network model and

the rigid rod model in that the fluid is locally anisotropic. Fluid motion is not continuous but occurs among discrete domains in a classical analogy to solid surface friction or superfluidity. Anderson (5) has proposed this model to describe large-scale density waves in smectic B liquid crystals. If one domain slides over another, two roughnesses encountering one another must either be completely overwhelmed by the forces driving them or must stop the motion entirely. A roughness cannot provide a continuous source of linear dissipation because any roughness that causes a purely elastic deformation does not dissipate energy. Instead, it returns as much mechanical energy to the lattice as was present in the original deformation. Viscous stress is thus viewed as the (shear rate dependent) force necessary to substantially kink or break those protein strands that extend from one solid domain to another. The effect that biologists call gelation is, presumably liquid crystal domain formation. This solid friction analogy is supported by the finding of ourselves and others (71) that the initial shear stress (analogous to static friction of solids) is always greater than the steady state stress (analogous to sliding friction of solids). Additional evidence for this model is shown in Fig. 24 in which actin and microtubule protein suspensions reveal distinct domains under polarized light in contradiction to the assumptions of the rigid rod model described above.

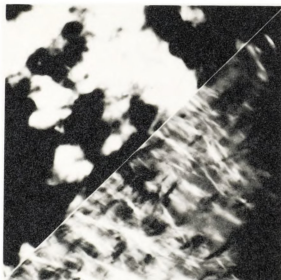
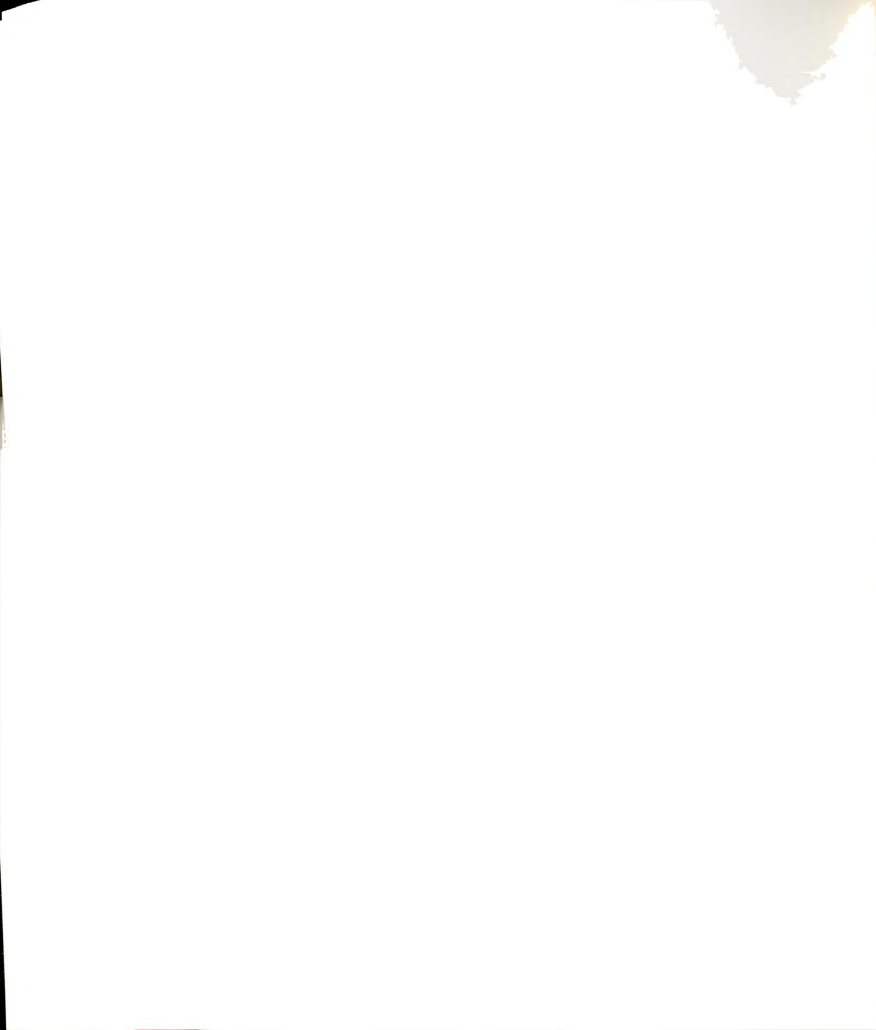
F-ACTIN**MICROTUBULES**

Figure 24. Polarization micrographs of suspensions of actin and microtubules.

The upper left micrograph is of F-Actin at 25 mg/ml. (Similar domains were seen at concentrations of 8 mg/ml but the birefringence was too dim to photograph successfully). The lower right micrograph is of microtubules at a concentration of 6 mg/ml.



APPENDICES



Appendix A. Method for analytical determination of neurite mechanical constants from observed distension behavior.

T = Tension held by neurite, To = non-distended neurite rest tension
 L = Neurite length, Lo = non distended neurite rest length

Short duration elastic extensions:

**** k1 = slope of Tension vs Length plot ****

Long duration V/E extension at equilibrium:

$$K(nrt) = (T_{eq} - T_o) / (L_{eq} - L_o)$$

$$1/K(nrt) = 1/k_1 + 1/k_2$$

**** k2 = 1/(1/Knrt - 1/k1) ****

Duing V/E distension:

portion of elongation due to spring 1 is Δx_1

by Hook's law $T - T_o = k_1 \times \Delta x_1$, therefore $\Delta x_1 = (T - T_o) / k_1$
 (spring 1 is "free")

portion of elongation due to Voight element is Δx_2

$$\Delta x_2 = (L - L_o) - \Delta x_1$$

$$T(\text{spring 2}) = k_2 \times \Delta x_2$$

$$\begin{aligned} \Delta x_2' &= \text{time rate of change of } x_2 \text{ (Voight element length)} \\ &= [\Delta x_2(\text{time2}) - \Delta x_2(\text{time1})] / (\text{time2} - \text{time1}) \end{aligned}$$

H = dashpot constant

$$T - T_o = k_1 \times \Delta x_1 = (k_2 \times \Delta x_2) + (H \times \Delta x_2')$$

**** H = [(T - T_o) - (k2 x Δx2)] / Δx2' ****

H is calculated for every time interval (2 mins) and averaged

To, k1, k2, Knrt and H are constants for a paticular neurite

Δx_1 , Δx_2 , $\Delta x_2'$ and T are all varying during an applied distension



Appendix B. Logic underlying the computer simulation based on our viscoelastic model for neurite distension.

The computer simulation is written in the APL programming language (STSC, Inc., Rockville, MD). String variables were created for the following parameters: **T** (neurite tension), **L** (neurite length), **F** (needle force), **B** (height of distension triangle, equivalent to distance "b" in figure 10), **X1** (length increase of spring 1 relative to its length at zero distension), **X2** (relative length of Voigt element) and **t** (simulation time). Individual string values represent that parameter's value as calculated over successive intervals in "simulated time". Constants were defined for the following parameters: **Lr** (neurite "rest" length: length at zero distension), **Tr** (neurite "rest" axial tension), **Fb** (beginning applied force held by the needle), **CAL** (needle calibration constant), **Tb** (beginning neurite axial tension), **K1** (spring 1 elastic modulus), **K2** (spring 2 elastic modulus), **H** (dashpot viscosity constant), **dt** (time interval between calculated values in "simulated time"), and **N** (number of time intervals calculated). Constants were given new values prior to each simulation run based on values from a particular long duration distension experiment

The computer simulation uses a numerical approximation method that requires small values for **dt** and large values for **N** to achieve satisfactory results. I typically used a



value of 3 (secs) for Δt which required a value of 600 for N to give a net simulation time of 30 minutes. Resulting simulation values were sequentially stored in the string variables. Every tenth value (time interval of 30 seconds) of the neurite tension variable (T) was plotted on the y-axis against every tenth value of the time variable (t) and connected with a smooth curve. This plot was combined with the actual tension-over-time data for the particular neurite distension to give each of the four graphs in figure 13.

The following paragraph states our viscoelastic model in mathematical terminology. A free spring (K_1) and a Voight element (a spring (K_2) in parallel with a dashpot (H)) are in series and therefore each continuously hold the entire neurite tension. A change in neurite axial tension (T) equals the product of the change in length of spring 1 (X_1) and its elastic modulus (K_1). Also, a change in neurite axial tension equals the sum of a) the product of the change in length of spring 2 (X_2) and its elastic modulus (K_2) and b) the product of the dashpot viscosity constant (H) and the time rate of change of dashpot length (\dot{X}_2).

This same relationship is expressed symbolically below. The string variable for tension is a series: $T[1]$, $T[2]$, $T[3]$, ... $T[N]$. $T[1]$ is neurite tension at 0 seconds (immediately following distension), $T[2]$ is neurite tension at 3 seconds, $T[3]$ is neurite tension at 6 seconds, etc. The same is true for the other string variables. The change

in neurite tension between arbitrary (i)th and (j)th values of T is represented as $T[j]-T[i]$. I can therefore represent the word description in the preceeding paragraph by the following equations:

$$T[j]-T[i] = (K1)(X1[j]-X1[i]) \quad \text{Equation 1}$$

$$T[j]-T[i] = (K2)(X2[j]-X2[i]) + H(X2[j]-X2[i]/(t[j]-t[i]))$$

Equation 2

----- IN REVIEW -----

Constants

L_r = neurite rest length (um)
 T_r = neurite rest tension (udynes)
 K_1 = elastic modulus of "free" spring 1 (udynes/um)
 K_2 = elastic modulus of Voight spring 2 (udynes/um)
 H = dashpot viscosity constant (udyne)(sec)/(um)
 CAL = needle calibration constant (udynes/um)
 dt = simulated time increment (secs)
 N = number of computer iterations

Initial Conditions

F_b = initial applied lateral needle force (udynes)
 T_b = initial resulting neurite axial tension (udynes)



String Variables

B[i] = resulting lateral displacement distances

(height of distension triangle in um)

T[i] = resulting neurite tensions over time (udynes)

L[i] = resulting neurite lengths over time (um)

X1[i] = resulting spring 1 lengths over time

(relative to its "rest" length in um))

X2[i] = resulting Voight element lengths over time

(relative to its "rest" length in um)

t[i] = simulated time values in multiples of **dt** (secs)

----- PROGRAM LOGIC -----

The following assumptions are made for all
instantaneous changes in neurite tension (including the
initial distension):

- a) only spring 1 length (**X1**) changes.
- b) spring 2 and the dashpot length (**X2**) do not respond
instantaneously. Their response requires some
finite amount of time (**dt**) to pass.

Program Steps

- 1) set all string variable values to zero, the iteration
counter (**i**) to 1, and all constants to their
respective values.
- 2) set **F[1] = Fb** and **T[1] = Tb**.



- 3) let spring 1 length ($X1$) increase in response to initial increase in neurite tension.

$$X1[i] = (Tb - Tr) / K1 \quad (\text{from equation 1 above})$$

- 4) let neurite length increase by this amount

$$L[i] = Lr + X1[1]$$

START OF LOOP:

- 5) let iteration counter increase by 1

$$i = i + 1$$

- 6) let some small finite amount of time (dt) pass

$$t[i] = t[i-1] + dt$$

(hold neurite tension and therefore spring 1 length constant for now)

- 7) let Voight element length ($X2$) increase

$$X2[i] = \frac{(T[i-1] - T[i])(dt) + (H)(X2[i-1])}{(K2)(dt) + H}$$

(this is derived by solving equation 2 above for $X2$)

- 8) let neurite length (L) increase by this amount

$$L[i] = Lr + X1[i-1] + X2[i]$$

- 9) as the neurite elongates, let triangle height (B) increase...

$$B[i] = (0.5)(L[i]^2 - Lr^2)^{0.5}$$

(this is derived by Pathagorean thereom)

- 10) ... and needle force (F) diminish

$$F[i] = F[i-1] - (CAL)(B[i] - B[i-1])$$

- 11) as a result, let neurite tension (T) fall

$$T[i] = (F[i])(L[i]) / 4(B[i])$$

(this equation was derived in Chapter 1)

12) let spring 1 length (X1) decrease to in response to lower neurite tension

$$X1[i] = (T[i] - Tr) / K1 \quad (\text{from equation 1 above})$$

13) let neurite length (L) decrease by this amount (a small value compared to the increase in step 8).

$$L[i] = Lr + X1[i] + X2[i]$$

14) using new values for neurite length (L) and tension (T), return to step 5) and do this loop until total elapsed time is sufficient to reach plateau values for L and T. This effectively means to adjust the value of N.

APL Program Code

```
[0] TEN4
[1] i←1
[2] T[1]←Tb
[3] X1[1]←(T[1]-Tr)÷K1
[4] X2[1]←0
[5] L[1]←Lr+X1[1]
[6] F[1]←Fb
[7] B[1]←0.5×((L[1]×2)-Lr×2)×0.5
[8] START:i←i+1
[9] X2[i]←(((T[i-1]-Tr)×dt)+H×X2[i-1])÷H+K2×dt
[10] L[i]←Lr+X1[i-1]+X2[i]
[11] B[i]←0.5×((L[i]×2)-Lr×2)×0.5
[12] F[i]←F[i-1]-CAL×(B[i]-B[i-1])
[13] T[i]←(F[i]×L[i])÷(4×B[i])
[14] X1[i]←(T[i]-Tr)÷K1
[15] L[i]←Lr+X1[i]+X2[i]
[16] →(i<N)ρSTART
```


LITERATURE CITED



LITERATURE CITED

1. Abercrombie, M. 1982. The crawling movement of metazoan cells. In: Cell Behavior. edited by R. Bellairs, A. Curtis, and G. Dunn. Cambridge: Cambridge University Press, pp. 19-48.
2. Alberts, B.M., D. Bray, J. Lewis, M. Raff, K. Roberts, and J.D. Watson. 1989. Molecular Biology of the Cell. 2nd Ed. New York: Garland Publishing.
3. Albrecht-Buhler, G. 1987. Role of cortical tension in fibroblast shape and movement. Cell Motility and Cytoskeleton 7: 54-67.
4. Aletta, J.M. and L.A. Greene. 1987. Sequential phosphorylation of chactin microtubule-associated proteins is regulated by the presence of microtubules. J. Cell Biol. 105: 277-290.
5. Anderson, P.W. 1984. Basic Notions in Condensed Matter Physics. Menlo Park, CA: Benjamin-Cummings Pub. Co., pp. 159-164.
6. Bell, E., B. Ivarsson, and C. Merrill. 1979. Production of a tissue-like structure by contraction of collagen lattices by human fibroblast of different proliferative potential in vitro. Proc. Natl. Acad. Sci., U.S.A. 76: 1274-1278.
7. Bird, R.B., R.C. Armstrong, and O. Hassenagen. 1977. Dynamics of Polymer Liquids. New York: Wiley.
8. Black, M.M. and R.J. Lasek. 1980. Slow components of axonal transport: Two cytoskeletal networks. J. Cell Bio. 86: 616-622.
9. Bray, D. 1979. Mechanical tension produced by nerve cells in tissue culture. J Cell Sci 37: 391-410.
10. Bray, D. 1982. Filopodial contraction and growth cone guidance. In: Cell Behavior. edited by R. Bellair, A. Curtis, and G. Dunn. Cambridge: Cambridge University Press.
11. Bray, D. 1984. Axonal growth in response to experimentally applied tension. Develop. Biol. 102: 379-389.
12. Bray, D. 1987. Growth cones: do they pull or are they pushed?. Trends in Neurosci. 10: 431-434.
13. Bray, D. and D. Gilbert. 1981. Cytoskeletal elements in neurons. Ann Rev Neuroscience 4: 505-523.
14. Bray, D., C. Thomas, and G. Shaw. 1978. Growth cone formation in cultures of sensory neurons. Proc. Natl. Acad. Sci. USA. 75: 5226-5229.
15. Bray, D. and J.G. White. 1988. Cortical flow in animal cells. Science 239: 883-888.



16. Bunge, M.B., M.I. Johnson, and V.J. Argiro. 1983. Studies of regenerating nerve fibers and growth cones. In: *Spinal Cord Reconstruction*. edited by C. Kao, R.P. Bunge, and P.J. Reiner. New York: Raven Press, pp. 99-120.
17. Buxbaum, R.E., T. Dennerll, S. Weiss, and S.R. Heidemann. 1987. F-actin and microtubule suspensions as indeterminate fluids. *Science* 235: 1511-1514.
18. Buxbaum, R.E. and S.R. Heidemann. 1988. A thermodynamic model for force integration and microtubule assembly during axonal elongation. *J. Theor. Biol.* 134:379-390.
19. Campenot, R.B. 1977. Local control of neurite development by nerve growth factor. *Proc. Natl. Acad. Sci. USA* 74: 4516-4519.
20. Campenot, R.B. 1984. The regulation of nerve fiber length by intercalated elongation and retraction. *Devel. Brain Res.* 20: 149-154.
21. Cande, W.Z., J. Snyder, D. Smith, K. Summers, and J.R. McIntosh. 1974. A functional mitotic spindle prepared from mammalian cells in culture. *Proc. Natl. Acad. Sci. USA* 71: 1559-1563.
22. Cole, K.S. 1932. Surface forces of the Arbacia egg. *J. Cell Comp. Physiol.* 1: 1-19.
23. Cooper, J.A. 1987. Effects of cytochalasin and phalloidin on actin. *J. Cell Biol.* 105: 1473-1478.
24. Corvaja, N., A. DiLuzio, S. Biocca, A. Cattaneo, and P. Callissano. 1982. Morphological and ultrastructural changes in PC 12 pheochromocytoma cells induced by combined treatment with taxol and NGF. *Exp. Cell Res.* 142: 385-395.
25. Cowan, W.M., J.W. Fawcett, D.D.M. O'Leary, and B.B. Stanfield. 1984. Regressive events in neurogenesis. *Science* 225: 1258-1265.
26. Crick, F.H.C. and A.F.W. Hughes. 1950. The physical properties of cytoplasm: a study by means of the magnetic particle method. *Exp. Cell. Res.* 1: 37-80.
27. Daniels, M. 1975. The role of microtubules in the growth and stabilization of nerve fibers. *Ann NY Acad Sci* 253: 535-544.
28. Darnell, J., H. Lodish, and D. Baltimore. 1986. *Molecular Cell Biology*. New York: Scientific American Books.
29. DeBrabander, M., G. Guens, F. Van de Viere, F. Thone, F. Aerts, L. Desplanter, J. DeCree, and M. Borgers. 1977. The effects of R 17934, a new antimicrotubular substance, on the ultrastructure of neoplastic cells in vivo. *Eur. J. Cancer* 13: 511-528.



30. Dennerll, T.J., Joshi, H.C., Steel, V.L., Buxbaum, R.E., and Heidemann, S.R. 1988. Tension and compression in the cytoskeleton of PC-12 neurites II: Quantitative measurements. *J. Cell Biol.* 107: 665-674.
31. Denny, M.W. and J.M. Gosline. 1980. *J. Exp. Med.* 88: 375.
32. Doi, M. and S.F. Edwards. 1978. Dynamics of rod-like macromolecules in concentrated solution, part 2. *J. Chem. Soc. Faraday Trans. II* 74: 918-932.
33. Forscher, P. and S.J. Smith. 1988. Actions of cytochalasins on the organization of actin filaments and microtubules in aneuronal growth cone. *J. Cell Biol.* 107: 1505-1516.
34. Fuller, R.B. 1961. Tensegrity. *Portfolio and Artnews Annual* 4: 112-127.
35. George, E.B., B.F. Schneider, R.J. Lasek, and M.J. Katz. 1988. Axonal shortening and the mechanisms of axonal motility. *Cell Motility Cytoskeleton* 9: 48-59.
36. Goldberg, D.J. and D.W. Burmeister. 1986. Stages in axon formation: Observation of growth of Aplysia axons in culture using video-enhanced contrast-differential interference contrast microscopy. *J. Cell Biol.* 103: 1921-1931.
37. Graessley, W.W. 1965. Molecular entanglement theory of flow behavior in amorphous polymers. *J. Chem. Physics* 43: 2696-2703.
38. Graessley, W.W. 1967. Viscosity of entangling polydisperse polymers. *J. Chem. Physics* 47: 1942-1953.
39. Harris, A.K. 1982. Traction and its relations to contraction in tissue cell locomotion. In: *Cell Behavior*. edited by R. Bellairs, A. Curtis, and G. Dunn. Cambridge University Press, Cambridge.
40. Heidemann, S.R., H.C. Joshi, A. Shechter, J.R. Fletcher, and M. Bothwell. 1985. Synergistic effects of cyclic AMP and nerve growth factor on neurite outgrowth and microtubule stability. *J. Cell Biol.* 100: 916-927.
41. Heidemann, S.R., P. Lamoureux, and R.E. Buxbaum. 1988. Neurites of chick sensory neurons can generate tension in the absence of growth cone motility. *J. Cell Biol.* 107: 128a.
42. Heuser, J.E. and M.W. Kirschner. 1980. Filament organization revealed in platinum replicas of freeze dried cytoskeletons. *J. Cell Biol.* 86: 212-234.
43. Hill, T.L. and M.W. Kirschner. 1982. Bioenergetic and kinetics of microtubule and actin filament assembly-disassembly. *Int Rev Cytol* 78: 1-125.
44. Hiramoto, Y. 1963. Mechanical properties of sea urchin eggs. *Exp. Cell Res.* 32: 59-75.

45. Hiramoto, Y. 1969. Mechanical properties of the protoplasm of the sea urchin egg. *Exp. Cell Res.* 56: 201-208.
46. Hiramoto, Y. 1970. Rheological properties of sea urchin eggs. *Biorheology* 6: 201-234.
47. Hirokawa, N. 1982. Cross linker system between neurofilaments, microtubules and membranous organelles revealed by the quick freeze, deep etch method. *J. Cell Biol* 94: 129-142.
48. Hoffman, P.N. and R.J. Lasek. 1975. The slow component of axonal transport. Identification of major structural polypeptides of the axon and their generality among mammalian neurons. *J. Cell Biol.* 66: 351-366.
49. Ingber, D.E. and J. Folkman. 1988. Tension and compression as basic determinants of cell form and function: Utilization of a cellular tensegrity mechanism. In: *Cell Shape: Determinants, Regulation and Regulatory Role.* edited by W.D. Stein and F. Bronner. Orlando: Academic Press.
50. Ingber, D.E. and J.D. Jamieson. 1985. Cells as tensegrity structures: Architectural regulation of histodifferentiation by physical forces transduced over basement membrane. In: *Gene Expression during Neural and Malignant Differentiation.* edited by L.C. Anderson, C.G. Gahnberg, and P. Ekblom. New York: Academic Press.
51. Jacobs, J.R. and J.K. Stevens. 1986. Experimental modification of PC12 neurite shape with the microtubule-depolymerizing drug nocodazole: a serial electron microscopic study of neurite shape control. *J. Cell Biol.* 103: 907-916.
52. Jain, S. and C. Cohen. 1981. Rheology of rodlike macromolecules in semidilute solutions. *Macromolecules* 14: 759-765.
53. Joshi, H.C., D. Chu, R.E. Buxbaum, and S.R. Heidemann. 1985. Tension and Compression in the Cytoskeleton of PC 12 Neurites. *J. Cell Biol.* 101: 697-705.
54. Kamiya, N. 1981. Physical and chemical basis of cytoplasmic streaming. *Ann. Rev. Plant Physiol.* 32: 205-236.
55. Katz, M.J., E.B. George, and L.J. Gilbert. 1984. Axonal elongation as a stochastic walk. *Cell Motility* 4: 351-370.
56. King, M. and P.T. Macklem. 1977. Rheological Properties of microliter quantities of mucus. *J. Appl. Physiol. Resp. Environ. Exercise Physiol.* 42: 797-802.
57. Kolega, J. 1986. Effects of mechanical tension on protrusive activity and microfilament and intermediate filament organization in an epidermal epithelium in culture. *J. Cell Biol.* 102: 1400-1411.



58. Laemmli, U.K. 1970. Cleavage of structural proteins during the assembly of the head of bacteriophage T4. *Nature* 227: 680-685.
59. Lamoureux, P., R.E. Buxbaum, and S.R. Heidemann. 1989. Direct evidence that growth cones pull. *Nature* (London) : submitted.
60. Landis, S.C. 1983. Neuronal growth cones. *Ann Rev Physiol* 45: 567-580.
61. Letourneau, P.C. 1975. Cell-to-substratum adhesion and guidance of axonal elongation. *Dev Biol* 44: 92-101.
62. Letourneau, P.C. 1981. Immunocytochemical evidence for colocalization in neurite growth cones of actin and myosin and their relationship to cell substratum adhesions. *Developmental Biol.* 85: 113-122.
63. Letourneau, P.C. 1982. Nerve fiber growth and its regulation by extrinsic factors. In: *Neuronal Development*. edited by N.C. Spitzer. New York: Plenum Press.
64. Letourneau, P.C. and A.H. Ressler. 1984. Inhibition of neurite initiation and growth by taxol. *J. Cell Biol.* 98: 1355-1362.
65. Letourneau, P.C., T.A. Shattuck, and A.H. Ressler. 1987. "Pull" and "push" in neurite elongation: Observations on the effects of different concentrations of cytochalasin B and taxol. *Cell Motility Cytoskeleton* 8: 193-209.
66. Levin, A. and J. Wyman. 1927. The viscous elastic properties of muscle. *Proc. Roy. Soc. B* 101: 218-43.
67. Lintilhac, P.M. and T.B. Vesecky. 1984. Stress-induced alignment of division plane in plant tissues grown in vitro. *Nature* 307: 363-364.
68. MacLean-Fletcher, S. and T.D. Pollard. 1980. Identification of a factor in conventional muscle actin preparations which inhibits actin filament self-association. *Biochem. Biophys. Res. Comm.* 96: 18-27.
69. MacLean-Fletcher, S.D. and T.D. Pollard. 1980. Vicometric analysis of the gelation of *Acanthamoeba* extracts and purification of two gelation factors. *J. Cell Biol.* 85: 414-428.
70. Marsh, L. and P.C. Letourneau. 1984. Growth of neurites without filopodial or lamellipodial activity in the presence of cytochalasin B. *J. Cell Biol.* 99: 2041-2047.
71. Maruyama, K., M. Kaibara, and E. Fukuda. 1974. Rheology of actin, 1. Network of F-actin in solution. *Biochim. Biophys. Acta* 371: 20-29.
72. Meissner, J. 1972. Modifications of the Weissenberg rheogoniometer for measurement of transient rheological properties of molten polyethylene. *J. Appl. Polymer Sci.* 16: 2877-2899.



73. Mitchison, J.M. and M.M. Swann. 1954. The mechanical properties of the cell surface. I. The cell elastimeter. *J. Exp. Biol.* 31: 443-460.
74. Mitchison, T. and M. Kirschner. 1988. Cytoskeletal dynamics and nerve growth. *Neuron* 1: 761-772.
75. Mizushima-Sugano, J., T. Maeda, and T. Miki-Nomura. 1983. Flexural rigidity of singlet microtubules estimated from statistical analysis of their contour lengths and end-to-end distances. *Biochim et Biophys Acta* 755: 257-262.
76. Morris, J.R. and R.J. Lasek. 1982. Stable polymers of the axonal cytoskeleton: the axoplasmic ghost. *J Cell Biol* 92: 192-198.
77. Nemoto, I. 1982. A model of magnetization and relaxation of ferrimagnetic particles in the lung. *Inst. Electr. Electron. Eng. Trans. Biomed. Eng.* 29: 745-752.
78. Nicklas, R.B. 1983. Measurements of the force produced by the mitotic spindle in anaphase. *J. Cell Biol.* 97: 542-548.
79. Opperman, A. and B. Jaberg. 1985. Rheological properties of liver actin solutions. *Rheol. Acta* 24: 525-529.
80. Pasternak, C. and E.L. Elson. 1985. Lymphocyte mechanical response triggered by cross-linking surface receptors. *J. Cell Biol.* 100: 860-872.
81. Peterson, N.O., W.B. McConnaughey, and E.L. Elson. 1982. Dependence of locally measured cellular deformability on position on the cell, temperature and cytochalasin B. *Proc. Natl. Acad. Sci. USA* 79: 5327-5331.
82. Porter, K.R. 1984. The cytomatrix: A short history of its study. *J. Cell Biol.* 99 Supp: 3s-12s.
83. Purcell, E.M. 1977. *Am. J. Phys.* 45: 3.
84. Purves, D. and J.W. Lichtman. 1985. *Principles of Neuronal Development*. Sunderland, Mass.: Sinauer Associates.
85. Rappaport, R. 1967. Cell division: Direct measurement of maximum tension exerted by furrow of echinoderm eggs. *Science* 167: 1241-1242.
86. Rebhun, L.I. 1972. *Int. Rev. Cytol.* 32: 92.
87. Rockwell, M.A., M. Fechheimer, and D.L. Taylor. 1984. A comparison of methods used to characterize gelation of actin in vitro. *Cell Motility* 4: 197-213.
88. Sato, M., G. Leimbach, W.H. Schwartz, and T.D. Pollard. 1985. Mechanical Properties of Actin. *J. Biol. Chem.* 260: 8585-8592.

89. Sato, M., W.H. Schwartz, and T.D. Pollard. 1987. Dependence of the mechanical properties of actin/actinin gels on deformation rate. *Nature* 325: 828-830.
90. Sato, M., T.Z. Wong, and R.D. Allen. 1983. Rheological properties of living cytoplasm: endoplasm of *Physarum plasmodium*. *J. Cell Biol.* 97: 1089-1097.
91. Schiff, P.B., J. Fant, and S.B. Horwitz. 1979. Promotion of microtubule assembly in vitro by taxol. *Nature (Lond.)* 277: 665-667.
92. Schliwa, M. 1982. Action of cytochalasin D on cytoskeletal networks. *J. Cell Biol.* 92: 79-91.
93. Schliwa, M., K.B. Pryzwansky, and J. Van Blerkom. 1982. Implications of cytoskeletal interactions for cellular architecture and behavior. *Phil. Trans. R. Soc. Lond. B* 299: 199-205.
94. Schnapp, B.J. and T.S. Reese. 1982. Cytoplasmic structure in rapid frozen axons. *J Cell Biol* 94: 667-679.
95. Schroeder, T.E. 1981. The origin of cleavage in dividing eggs. *Exp. Cell Res.* 134: 231-240.
96. Seifriz, W. 1942. *The Structure of Protoplasm*. Ames, Iowa: Iowa State College Press.
97. Shelanski, M.L., F. Gaskin, and C.R. Cantor. 1973. Microtubule assembly in the absence of added nucleotides. *Proc. Natl. Acad. Sci. USA* 70: 765-768.
98. Solomon, F. and M. Magendantz. 1981. Cytochalasin separates microtubule disassembly from loss of asymmetrical morphology. *J. Cell Biol.* 89: 157-161.
99. Solomon, F., M. Magendantz, and A. Salzman. 1979. Identification with microtubules of one of the microtubule-associated proteins. *Cell* 18: 431-438.
100. Spero, D.A. and F.J. Roisen. 1985. Neuro-2a neuroblastoma cells form neurites in the presence of taxol and cytochalasin D. *Dev. Br. Res.* 23: 155-159.
101. Spudich, J.A. and S. Watt. 1971. The regulation of rabbit skeletal muscle contraction. I. Biochemical studies of the interaction of the tropomyosin-troponin complex with actin and proteolytic fragments of myosin. *J. Biol. Chem.* 246: 4866-4871.
102. Stossel, T.P. 1984. Contribution of actin to the structure of the cytoplasmic matrix. *J. Cell Biol.* 99: 155-215.

103. Sung, K.P., W. Schmid-Schonbein, R. Skalak, U. Schuessler, U. Shunichi, and S. Chien. 1982. Influence of physiochemical factors on rheology of human neutrophils. *Biophys. J.* 39: 101-106.
104. Takeuchi, S. 1979. Wound healing in the cornea of the chick embryo. IV Promotion of the migratory activity of isolated corneal epithelium in culture by the application of tension. *Dev. Biol.* 70: 232-240.
105. Taylor, D.L. and J.S. Condeelis. 1979. Cytoplasmic structure and contractility in amoeboid cells. *Int. Rev. Cytol.* 56: 57-144.
106. Tomasek, J.J. and E.D. Hay. 1984. Analysis of the role of microfilaments and microtubules in acquisition of biopolarity and elongation of fibroblasts in hydrated collagen gels. *J. Cell Biol.* 99: 536-549.
107. Trinkaus, J.P. 1984. *Cells into Organs*, 2nd Edition. Prentice Hall Inc., Englewood Cliffs, NJ.
108. Trinkaus, J.P. 1985. Further thoughts on directional cell movement during morphogenesis. *J. Neurosci. Res.* 13: 1-19.
109. Valberg, P.A. and Albertini, D.F. 1985. Cytoplasmic motions rheology and structure probed by a novel magnetic particle method. *J Cell Biol* 101: 130-140.
110. Vandenburg, H.H. 1982. Dynamic mechanical orientation of skeletal myofibers in vitro. *Dev. Biol.* 93: 438-443.
111. Weingarten, M.W., M. Suter, D. Littman, and M.W. Kirschner. 1974. Properties of the depolymerization products of microtubules from mammalian brain. *Biochemistry* 13: 5529-5537.
112. Weiss, P. 1941. Nerve Pattern: The mechanics of nerve growth. *Growth (Suppl. Third Growth Symp.)* 5: 163-203.
113. Willard, M., W.M. Cowan, and P.R. Vagelos. 1974. The polypeptide composition of intra-axonally transported proteins: Evidence for four transport velocities. *Proc. Natl. Acad. Sci. USA* 71: 2183-2187.
114. Williams, R.C. and H.W. Detrich. 1979. Separation of tubulin from microtubule-associated proteins on phosphocellulose. Accompanying alterations in concentrations of buffer components. *Biochemistry* 18: 2499-2503.
115. Wolosewick, J.J. and K.R. Porter. 1979. The microtrabeculae lattice of the cytoplasmic ground substance: artifact or reality. *J. Cell Biol.* 82: 114-139.
116. Yagi, K. 1961. The mechanical and colloidal properties of Amoeba protoplasm and their relations to the mechanism of amoeboid movement. *Exp. Biochem. Physiol.* 3: 73-91.



117. Yamada, K.M., B.S. Spooner, and N.K. Wessels. 1970. Axon growth: role of microfilaments and microtubules. *Proc. Natl. Acad. Sci. USA* 66: 1206-1212.
118. Yanagida, T. and F. Oosawa. 1978. Polarized fluorescence from e-ADP incorporated into F-actin in a myosin free single fiber: Conformation of F Actin and changes induced in it by heavy meromyosin. *J. Mol. Biol.* 126: 507-524.
119. Zaner, K.S. and T.P. Stossel. 1982. Some perspectives on the viscosity of actin filaments. *J. Cell Biol.* 93: 987-991.
120. Zaner, K.S. and T.P. Stossel. 1983. Physical basis of the rheological properties of F-actin. *J Biol Chem* 258: 11004-11009.



MICHIGAN STATE UNIV. LIBRARIES



31293006257095